2017

A Study of Alkali-Resistant Materials for Use in Atomic Physics Based Systems

Aaron Thomas Fletcher
Wright State University

A STUDY OF ALKALI-RESISTANT MATERIALS FOR USE IN ATOMIC PHYSICS BASED SYSTEMS

A thesis submitted in partial fulfillment

of the requirements for the degree of

Master of Science

By

AARON THOMAS FLETCHER

B.S., Wright State University, 2015

2017

Wright State University

WRIGHT STATE UNIVERSITY

GRADUATE SCHOOL

July 24, 2017

I HEREBY RECOMMEND THAT THE THESIS PREPARED UNDER MY SUPERVISION BY Aaron Thomas Fletcher **ENTITLED** A Study of Alkali-Resistant Materials for Use in Atomic Physics Based Systems **BE ACCEPTED IN PARTIAL FULFILLMENT OF THE REQUIREMENTS FOR THE DEGREE OF** Master of Science.

_____

Gregory Kozlowski, Ph.D.

Thesis Director

_____

Jason Deibel, Ph.D.

Chair, Physics Department

College of Science and Mathematics

Committee on Final Examination

_____

Gregory Kozlowski, Ph.D.

_____

Steven Fairchild, Ph.D.

_____

David Turner, Ph.D.

_____

Robert Fyffe, Ph.D.
Vice President for Research and
Dean of the Graduate School

ABSTRACT

Fletcher, Aaron Thomas M.S. Department of Physics, Wright State University, 2017. A Study of Alkali-Resistant Materials for Use in Atomic Physics Based Systems.

Due to shortcomings in emerging alkali-based atomic physics based systems, a need to investigate alkali resistant materials has arisen. There is interest in alkali based systems such as atomic clocks and diode pumped alkali laser (DPAL) systems. In the case of atomic clocks and DPALs, alkali metal vapor, such as Rb, is the active part of the systems. The alkali vapor is confined in some manner of housing, but the transmission of electromagnetic radiation is required in the cells. This requires the incorporation of windows into the cell. The current window material, however, have been shown to degrade over time, thus reducing the effectiveness of these systems. It is believed that the alkali atoms diffuse into the bulk of the housing material. This diffusion results in changes of optical and, in some cases, structural properties of the material. These changes lead to the degradation of window materials in these alkali-based systems.

In an effort to improve the longevity of alkali-based systems, a material study was conducted to identify window material that could resist diffusion-based changes in optical properties. Candidate materials were selected based on their structure, optical properties, and/or density. All candidate materials underwent baseline characterization. Baseline characterization techniques included atomic force microscopy, spectrophotometry, reflectometry, ellipsometry, and X-ray diffraction spectroscopy. Once baseline data was collected, the candidate materials were exposed to Rb at high temperatures for an extended period of time to simulate atomic physics devices. Exposure was achieved by heating the Rb source to ~ 550 °C while the candidate materials were kept at ~ 450 °C. This created a 100 °C temperature gradient to thoroughly expose the materials to gaseous Rb. After exposure, the materials underwent the same analysis techniques to

ascertain the changes in structural and optical properties. Additionally, time of flight secondary ion mass spectroscopy depth profiling was conducted to quantitatively determine the depth of Rb into the bulk of the material.

The results of this research effort found that highly crystalline materials were capable of resisting alkali diffusion better than amorphous materials, often only tens of nm. Their optical properties were also relatively unchanged. Amorphous materials were not able to resist the diffusion of Rb; diffusion depths were shown to be on the order of microns. Based on this research effort, aluminum oxynitride, $MgAl_2O_4$, MgO, and ZrO_2 are being recommended as materials that will improve the longevity of emerging atomic physics systems. A vapor cell made from ZrO_2 was fabricated and is being evaluated for use in atomic clock systems. For DPAL systems, window materials will need to be further tested to determine whether it can resist the high fluence laser radiation after being exposed to Rb.

TABLE OF CONTENTS

LIST OF FIGURES

LIST OF TABLES

ACKNOWLEDGEMENTS

There are innumerably many people who have helped me during my career and deserve my thanks. While I regret I cannot address all of you individually to express the profound sense of gratitude I have, I will make an effort to thank some of you. For working with and guiding me in my research, I am eternally grateful to Drs. Gregory Kozlowski and David Turner. Dr. Steve Fairchild was instrumental in ensuring the research efforts were supported and funding was maintained. Drs. Tyson Back and Matt Lange also deserve no small amount of thanks for teaching me a variety of skills and knowledge.

There have been several instructors who took an interest in my learning and success. Drs. Jerry Clark, Jason Deibel, Brent Foy, Ivan Medvedev, and Mia Tian and Mr. Will Wagner of Wright State and Ms. Cynthia Lehmkuhle of Clark State all deserve recognition. Each of these instructors, while it may not have been apparent while I was taking their classes, significantly contributed to my comprehension of the challenging material they were tasked to impart and as such deserve a tremendous amount of thanks.

My mother Pauline and my father Scott provided me with love and support throughout my life – college being no exception. I would be nowhere without my parents. I want to thank my little sister, Audrey, for being supportive and for creating schematics used in this thesis.

My friends have been not only been supporting and encouraging, but have easily been the one of the best parts of my life thus far. For the enumerable times spent working together, talking, putting up with my antics, or simply having a good time together, I must thank my closest friends: Keith Adams, Jacob Artz, Erik Courter, Shannon Hennelly, Dan Huffman, Douglas Preston, Rachel Rai, Matt Rustad, and Andy and Ben Siva. It is my sincere hope that in the years to come all of us retains and strengthens the bonds of friendship we share.

Dedicated to my son, Sam

CHAPTER 1: INTRODUCTION

In emerging alkali metal based atomic physics systems, damage to windows housing gaseous alkali metals have shown that they degrade over a period of time which makes the transfer of these technologies from the laboratory to the field intractable. The goal of this research is twofold: first, identify the mechanism of degradation of window material in emerging atomic physics based systems and second, determine the optimal window material to improve the longevity of such systems. This Chapter will discuss the motivation behind this research and identify and expand upon the goals of this effort. Chapter 2 will discuss the emerging atomic physics systems this research aims to assist, namely diode pumped alkali lasers (DPAL) systems and atomic clocks. Chapter 3 will identify general properties of alkali resistance in materials as well as a list of candidate materials to be studied with a summary of their properties. Chapter 4 will explain the principles and application of the experimental measuring techniques used in this research. Chapter 5 will outline and explain the overall experimental approach. The results of the experimental data will be addressed in Chapter 6. Finally, Chapter 7 will discuss the significance of the results, make a formal recommendation of improved window materials, and outline future work.

1.1 Motivation

There are several vested interests in atomic physics based systems, specifically atomic clocks and DPALs. These systems, while distinct in function and, to an extent, operation as will be discussed in later sections, both rely on excited alkali vapor [1, 2]. Phenomena associated with energetic alkali metal vapor have led to several issues in these systems. In atomic clocks, the precision of the frequency standard decreases with prolonged use. This is believed to be caused by deterioration of window material within the atomic clock's resonance cavity. This decline in

effectiveness is a concern to those working to transition these systems from the laboratory to the field because, in some applications, (such as atomic clocks on satellites) replacing a failing atomic clock is not a viable option. Improving the longevity of atomic clocks is, therefore, an interest.

DPAL systems have been shown to hold promise for directed energy weapon (DEW) applications due to their ability to scale output power with the diode laser pump power, maintain high beam quality for extended continuous wave (CW) operation, and require low logistical support to operate. For these reasons, DPAL systems are being actively developed. A problem with these systems has been found: the window material used inside the laser cavity will catastrophically fail after approximately one month's use. Discoloration and physical etching are evident on the surface of the DPAL windows as is illustrated in Figure 1. These surface effects are believed to be either (or a combination of) a) the deposition of carbon from ethane decomposition on the surface of the DPAL window leaving soot, or b) the diffusion of Rb into the window material thereby altering the optical properties of the window itself. While both possibilities are actively being researched, the experiments and results presented herein will focus predominately on the diffusion of Rb into the window material in an effort to experimentally find a superior window material than quartz. The dramatic visual changes in the DPAL windows after catastrophic failure can be quantified by comparing their transmission as shown in Figure 2.

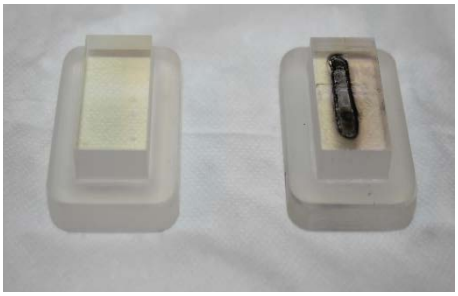

Figure 1*. A visual comparison of an unused (unexposed, left) and a damaged (exposed, right) DPAL window.*

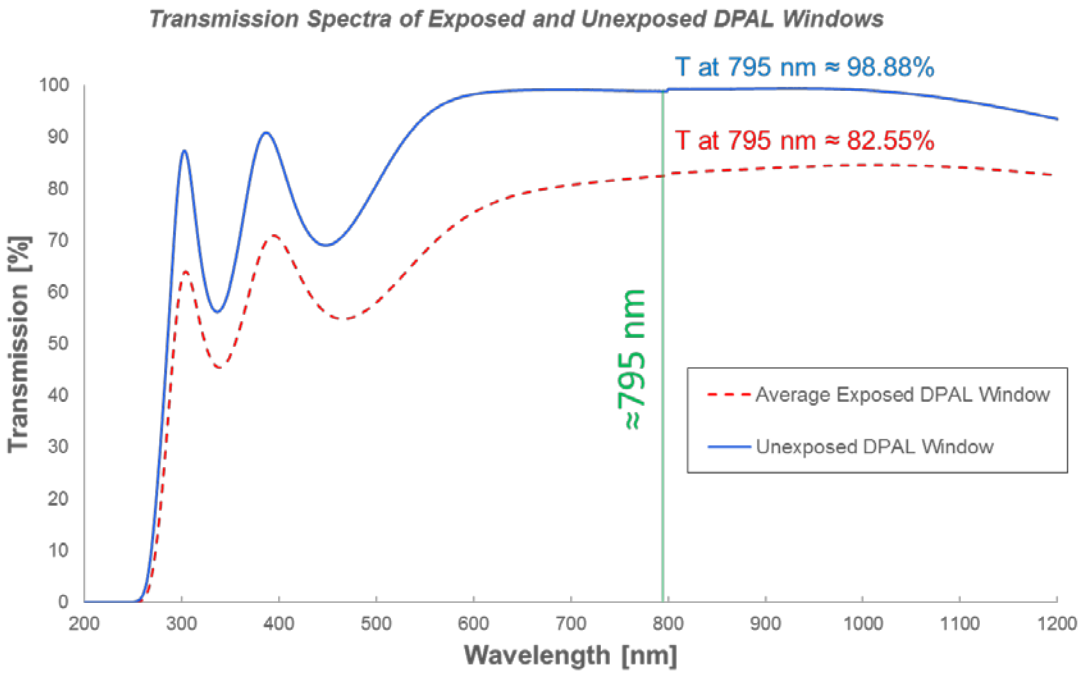

Figure 2. *Rough transmission measurements of DPAL windows before and after catastrophic failure.*

To understand these problems it is important to note that while both systems are distinct in function, they have a number of similarities in terms of operation and internal conditions. In addition to both systems relying on excited alkali metals, they both operate at elevated temperatures. The transmission of light through windows containing the alkali vapor is a requirement of both systems, even though the intensity of light is significantly higher in DPALs. Because of the similarities in system operation, it is believed that the issues plaguing atomic clocks and DPALs are similar and researching a means to improve the longevity of one system may also be a useful solution for the other. Atomic physics in general and specifics of both atomic clock and DPAL operating principles will be discussed in Chapter 2.

CHAPTER 2: BACKGROUND

2.1 Atomic Physics

Atomic physics generally refers to the study of an atom, its electrical structure, and associated transitions and emissions. This thesis will not delve into the considerable depth of the field of atomic physics as a tremendous amount of work done on the subject by Rutherford, Born, Fermi, Slater, Oppenheimer, Feynman, etc., and by the countless researchers who have spent their careers developing the field. However, a discussion will be given herein in an effort to provide a working knowledge of the phenomenon relevant to this research.

For purposes of this research effort, the focus of the introduction of atomic physics shall be on electron transitions and relaxations, the mechanisms that cause these phenomena, and the consequences thereof. When energy is exchanged between a source and an atom, it is possible for the atom to absorb that energy and move to an excited state if enough energy is transferred. Because of the propensity for any system to minimize its energy state and maximize entropy, the atom will not remain in an excited state for long and will relax to its lowest energy state if possible. Due to the law of energy conservation, however, the difference in energy between the excited state and the state to which the atom is falling to must be accounted for. If no collisions occur or other mechanisms exist to transfer energy, the energy from the difference in states will be expelled from the atom in the form of a photon whose frequency ν depends on the energy scaled by the inverse of Planck's constant h from the familiar Planck's equation, $\Delta E = h\nu$. The classical process of a photon being emitted when an atom will relax from an excited state to a lower state as described above is known as spontaneous emission.

Stimulated emission is a quantum mechanical phenomenon that provides the mechanism for lasers to emit radiation. While similar to spontaneous emission in some sense, stimulated

emission differs significantly from that classical effect. In stimulated emission, a photon will interact with an atom in an excited state. If the interacting photon corresponds to the energy gap between the excited state and a lower state, the original photon will continue on its path after interaction. There will however be an additional photon with the same frequency, phase, and direction that is generated by the excited atom or molecule thus effectively doubling the initial photon energy of the system, or amplifying the photon energy. This principle is the core mechanic behind all laser technology. Lasers function using the phenomena of stimulated emission coupled with a population of atoms or molecules that when more of these particles are in excited states than, for example, a ground state (this is called a population inversion) will release stimulated radiation as a spatially coherent beam of photons.

2.1.1 Atomic Clocks

Atomic clocks, like all other timekeeping devices, rely on a consistent, measurable frequency. Pendulum clocks, for example, can keep time based on the time it takes for the pendulum to swing to the point furthest from whence it started and to return to its origin. The frequency of the oscillation between the pendulum's extrema is and has been used to keep time. Because of external forces acting on a pendulum, the oscillations will eventually decay to an equilibrium position and stop moving. Because of these forces, the timekeeping ability of pendulum clocks is imprecise. Timing is an essential part in modern society and a need for accurate and precise timing is required. One of the most familiar uses of precision timing is the global positioning system (GPS).

GPS is a tool that is ubiquitous in commercial, government, and defense industries as well as at the individual level for social media and navigation. GPS is based on a constellation of satellites that orbit the Earth that are able to, in effect, triangulate the position of a GPS receiver

anywhere on or about the surface of the Earth. These satellites have this capability because of highly precise timing devices onboard them. A satellite is able to identify a point on the Earth's surface relative to its position. Its position is known based on the amount of time that has passed after it has passed directly over a point with a specific location on the ground. The timing between the satellite passing over points like this are critical in relaying accurate spatial about some point on Earth. If the timing system on the satellite has some difference between its own timing and timing on the ground, then inaccuracies in perceived position can occur. It is for this reason that not only accurate time keeping devices be installed on satellites, but they must be compact enough to minimize the logistical cost of launching the satellite into orbit.

Atomic clocks function by allowing gaseous alkali metal atoms to be excited and to allow them to relax and spontaneously emit a photon [3]. Generally speaking, there is an interrogation beam that will go into and through the alkali cloud. When the cloud is excited, the alkali will relax to its ground state emitting a photon. This fluorescence occurs at highly regular intervals and can be detected. The oscillation between the excited and ground state is highly periodic; cesium (Cs), used in the current atomic timing standard clocks, has a transition frequency of 9.192631770 GHz [3]. This highly precise periodicity allows for effective timekeeping.

Because the alkali metal is pumped by an external light source, there obviously must be a window that allows the transmission of that source into the cell. In order to maintain the longevity of the atomic clock, these windows must ensure that the pump beam reaches the alkali within the cell. Over time, however, the ability for these windows to ensure the transmission of light degrades which, in turn, results in inaccuracies and eventual failure of the atomic clock. The degradation of these windows is something worth investigating in order to improve the longevity of atomic clock systems. Additionally, there is work being done on alkali-earth based atomic clocks (e.g., Ca and

Sr) and the degradation of the cell windows and vapor cells as a whole is an impediment for such research [4]. Atomic clock windows and cell material, as was mentioned above, must allow for the transmission of the wavelength generated from transitions between ground and excited states. The wavelength of interest ranges from the UV (318 nm for Cs) to the visible (657 nm for Ca) for the clocks involved. These ranges are of great interest for this research.

2.1.2 Diode Pumped Alkali Lasers

DPAL systems are of great interest to many for high energy and DEW applications for several reasons. DPAL systems, by virtue of being a gas phase laser, are not plagued by heat buildup as severely as solid state lasers are [2]. This allows for better beam quality without degradation thereof due to thermal effects while in CW mode [5]. DPALs also have the ability to scale power outputs with relative ease due to the fact that they are pumped by a diode. DPAL power outputs can range from the sub kW to the MW output power regimes [5]. DPAL systems also have lower logistics costs when compared to other high power gas laser systems. Arguably the most appealing feature of DPAL systems of solid state lasers is the quantum efficiency; DPAL systems have quantum efficiency above 95% [2]. This is significant when compared to a typical Nd:YAG laser whose quantum efficiency is 76% [2]. This means that the ratio of input power to output power for DPALs is higher than that of typical Nd:YAG lasers.

This research effort deals predominately with Rb-based DLAP systems. These DPALs use a gaseous mix of Rb, He, and C_2H_6, as the gain medium for the laser system [6]. In order to maintain the gas phase of the Rb, the gain medium is kept at ~ 250 °C. Each of the gases has a specific role; Rb is the active lasing medium that is pumped by a 780 nm diode laser and is excited from the $^2S_{1/2}$ state to the $^2P_{3/2}$ state [2, 6]. From that state, the C_2H_6 will relax the excited Rb to

the $^2P_{1/2}$ state by collision where a population inversion will occur and the Rb will lase at 795 nm [6]. The helium is simply a buffer gas [5].

As with all high powered laser systems, maximizing output power is a high priority, particularly if the laser system is to be used in a DEW-type role. Because of this, the windows used to pass light from the gain medium to the outside environment must be as transmissive as possible at the output wavelength; in the case of Rb DPAL systems that wavelength is 795 nm [2]. Windows used in current Rb DPAL lasers are made of fused silica and have anti-reflective (AR) coatings on the surface in order to bring transmission as close to 100% as possible. As was shown earlier in this Section, these windows cannot withstand the high energy, caustic environments of DPAL systems for extended periods of time. The cause of the catastrophic failure of these windows is of paramount importance to this research.

2.2 Alkali Damage Mechanism

As it was alluded to earlier, both atomic clocks and DPALs have intrinsic issues associated with the use of alkali atoms, specifically in the degradation and ultimate failure of the systems' windows. This occurs when alkali metals diffuse into the bulk of a material and alter its optical properties [7]. Diffusion is frequently modeled by using Fick's laws. These laws are shown below (Eqs. (1) and (2)):

$$\vec{J} = -D\vec{\nabla}C \tag{1}$$

$$\frac{\partial C}{\partial t} = D\nabla^2 C \tag{2}$$

The above are Fick's first (Eq. (1)) and second (Eq. (2)) laws of diffusion where $\vec{J}$ is the mass flux vector, D is the diffusivity, and C is the concentration as a function of time and position.

Diffusion is often well modelled by the Fick's laws. There is, however, shortcoming. The diffusion of gaseous matter into solids is often difficult to calculate because of the unknown diffusivity. Diffusivity is given by Eq. (3) as follows

$$D = D_{\infty} e^{-E_A/k_B T} \tag{3}$$

Eq. (3) is known as the Arrhenius equation where D_{∞} is diffusivity at infinite temperature, E_A is the activation energy required for the gas to react with the bulk material, k_B is the Boltzmann constant, and T is absolute temperature. While the Arrhenius equation does provide the basis for determining the diffusivity, there are two variables that are not necessarily well known D_{∞} and E_A. Literature detailing D_{∞} and E_A for Rb – glass reactions are sparse and can vary greatly owing to the strong temperature dependence of the diffusivity and activation energy. This temperature dependence is not well described in literature and it is also difficult to account for local non-uniformities in material properties and how that effects thermal energy distribution. Furthermore, because many materials will need to be characterized solving the Arrhenius equation and applying the results to Fick's laws will require experimental data to solve accurately. Because of the need for experimentation, other methods for examining how diffusion occurs in window material will be explored instead of solving the Arrhenius equation and Fick's laws for each material studied.

In order to understand the mechanisms of alkali diffusion and damage without using the well-known Fick's laws, a search of literature for other explanations and approaches was conducted. It has shown that alkali metals, like Rb, have a propensity to "attack" materials – particularly oxides and halides, breaking bonds and forming alkali-oxide or alkali-halide compounds as the case may be [5, 7, 8]. Simulations and experiments have been conducted to describe physical mechanism by which alkali metals diffuse into bulk materials [7, 8]. Work by

Tilocca used Car–Parrinello Molecular Dynamics (MD) simulations to model trajectories of Na and Ca particles into amorphous glasses. Na diffusion in a silicate material is shown in Figure 3. Note that the Na atom is bonding to the oxygen molecules and pulls itself through the bulk of the material. The Na-O bonds and the breaking of metal-oxide (e.g., Si-O) are the mechanism by which alkali atoms migrate through a material.

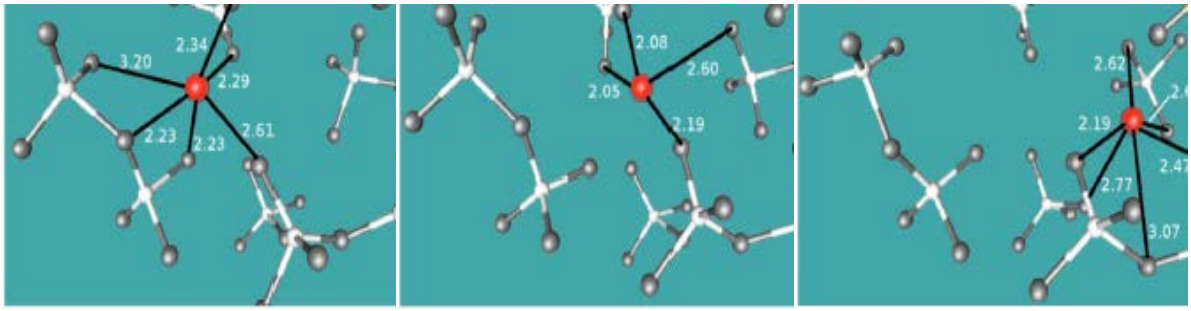

Figure 3. *Molecular Dynamics simulation done by Tilocca illustrating the diffusion of a Na (red) atom through a silicon (white) oxide (gray) cluster. Adapted from [8]*

A steady state thermodynamics argument made by Lau [7] shows that it is favorable for silicate glasses to be reduced by alkali metals as shown in Eqs. (4)−(6).

$$4Na + SiO_2 \rightarrow 2Na_2O + Si \qquad \Delta G > 0 \qquad (4)$$

$$2Na_2O + 4SiO_2 \rightarrow 2Na_2Si_2O_5 \qquad \Delta G < 0 \qquad (5)$$

$$4Na + 5SiO_2 \rightarrow 2Na_2Si_2O_5 + Si \qquad \Delta G < 0 \qquad (6)$$

Eq. (4) indicates that the reaction of Na with SiO_2 does not occur frequently since the Gibbs free energy is positive. Eqs. (5) and (6), however, show that when such a reaction as in Eq. (4) does occur, the reduction of the silicate and formation of alkali-silicate compounds occurs readily owing to a negative Gibbs free energy [7]. This process and the MD simulation show that it is relatively easy for metal-oxide materials to have alkali metals diffuse into them.

Diffusion, it is believed, precipitates in physical damage to the windows in atomic physics based systems. The amount of diffusion has previously been shown to have strong temperature dependence [9]. At temperatures below 200 °C, the diffusion goes as approximately the square root of temperature [9]. The diffusion can lead to discoloration, changes in optical properties and structure. If diffusion occurs under 200 °C, it is generally reversible in amorphous materials as bleaching agents can remove the diffused particles caught in the grain boundaries [7]. Above 200 °C, the diffusion rate increases and is roughly linear in terms of temperature and is a chemically limited process – that is bonds are being broken and reformed as the alkali atom diffuses through the bulk material [9]. This high temperature, chemically driven diffusion can also produce changes in optical properties and structure but these changes are largely irreversible.

For atomic clock applications, diffusion occurs and degrades the optical characteristics of the windows used to house the alkali vapor thereby reducing the effectiveness of atomic clocks. This is of particular concern in satellite-based atomic clocks as repair and replacement of damaged atomic clocks is not a viable option. The issue of diffusion is exacerbated in DPAL systems because the local changes in optical properties, specifically absorbance, leads to the previously mentioned catastrophic failure of DPAL windows. It is believed that the changes in absorption in the window leads to tremendous heat buildup as laser fluence on the order of kW/cm^2 attempt to pass through the window [5]. Because current materials used in atomic physics based systems are susceptible to alkali attack, i.e., diffusion, a rigorous study of materials that can resist such attack is described herein.

CHAPTER 3: MATERIALS

3.1 Alkali-resistant Materials

The study of materials that resist alkali damage has been of interest for some time, particularly in the concrete industry [10, 11, 12]. In that industry, high alkalinity leads to the degradation of concrete over time. In most modern concrete, there are silica fibers that reinforce the concrete, making it more durable [12]. Alkali metals, Na in particular, in aqueous solution attack these silica fibers which lead to irreparable damage in concrete. Cheng, et al. [12] developed a strategy to combat degradation of silica fibers by coating the fibers in zirconia. It was shown that zirconia-coated fibers resisted the damage caused by Na better than uncoated fibers; the damage analysis was done by visual inspection and comparison of the fibers using scanning electron microscopy (SEM) [12].

Other factors that resist aqueous alkali damage have been investigated: the density of amorphous glasses (e.g. silicates), temperature of the environment, and amount of surface area exposed to the alkali solution [13]. It is important to note that in DPALs and atomic clocks that an aqueous alkali is not present – the alkali is in gas phase. However, many of the materials that resist aqueous alkali solutions also resist diffusion of gaseous alkali as well [7]. The more densely packed the grains in polycrystalline material or the high degree of crystallinity are both major factors in a material's ability to resist [5, 7].

3.2 Candidate Materials

The materials used for this research were selected for a variety of reasons. These reasons were generally based on optical characteristics at 795 nm, density and/or degree of crystallinity, relative ease of fabrication, melting point (T_m), and ability to resist alkali damage and diffusion. This Section will discuss the materials that participated in this study. They are broken up into

amorphous, crystalline oxide, sapphire-like, Rb-based crystals, perovskite, and other crystalline materials.

3.2.1 Amorphous Materials

Even though literature suggests that amorphous materials are unlikely to be useful candidates for alkali resistance, several materials were analyzed anyway [7]. First, DPAL windows were acquired in order to ascertain what the current, ineffective windows' properties are and determine what should be avoided. While more detail about analysis on the DPAL window will be given later in this work, it should be noted that the DPAL windows have an anti-reflective (AR) coating of $MgF_2/Ta_2O_5/Al_2O_3$ on top of the bulk quartz.

Another amorphous material being tested is a commercially available glass made by Schott under their designation of 8436. Schott 8436 is advertised as an alkali-resistant glass and contains a small amount of ZrO_2 [14]. ZrO_2, as was mentioned earlier, is a material that can resist alkali metals. Small amounts (~ 3 atm. %) incorporated into a bulk glass has been shown to resist alkali metal diffusion and damage [15]. Schott only manufactures 8436 in tubing so it was necessary to fabricate a more disk-like sample. This was done by pulverizing the tubing and melting it into a puck, then polish the puck until it was not opaque.

The other amorphous glass tested was a tantalum flint glass known as TAFD-40. Tantalum-flint glasses are used commonly in optics and windows. TAFD-40 is a particularly dense tantalum flint glass and as such should be better at resisting alkali diffusion even though it is an amorphous material. If TAFD-40 is successful at resisting alkali diffusion, then other dense amorphous materials could become candidates for alkali resistant windows. This could be advantageous as amorphous materials are typically easier and less expensive to produce than single crystals. TAFD-40 also has reasonable optical properties at the desired wavelength. Some of the handbook physical

properties which include melting temperature T_m, initial transmission T_i and mass density ρ are summarized in Table 1.

Table 1. *Physical properties of amorphous materials.*

MATERIAL	Structure	T_m [°C]	T_i [%] (at λ [nm])	ρ [g/cm^3]
Fuse Silica[16]	Amorphous	1728	85 (795)	2.65
Schott 8436[14]	Amorphous	1100	> 80 (visible)	2.77
TAFD-40[17]	Amorphous	771	99.8 (800)	5.19

3.2.2 Crystalline Oxides

As discussed above, highly crystalline materials have been shown to better resist alkali diffusion and damage. ZrO_2 was already mentioned explicitly because of its ability to resist alkali damage in the concrete industry. In addition to its intrinsic ability to resist alkali damage, ZrO_2 has high transmission in the region of interest and can be grown with high crystallinity and in large pieces. Additionally, ZrO_2 has a high melting point which can protect it from both heated environments of atomic clocks and, ideally, from high fluence laser radiation.

Bismuth germinate $Bi_4Ge_3O_{12}$ (BGO) and lutetium-yttrium oxyorthosilicate $Lu_{2(1-x)}Y_{2x}SiO_5$ (LYSO) are a cubic structured material that is commonly used as a scintillator. Both of these materials are densely packed crystal whose optical properties are not unreasonable for the work being conducted. Additionally, both BGO and LYSO have high mechanical strength which will be useful for creating window and vapor cell materials.

Magnesium oxide is a very common material in optics and can be made with a high degree of crystallinity and is highly transparent at the desired wavelength. Because of its ubiquity in the optical industry, the manufacturing of MgO windows or small vapor cells would not be excessively

difficult to accomplish. The bond between Mg and O is also fairly strong which should discourage the diffusion of alkali metals through the MgO network.

ThO_2 is a material with one of the highest melting points of any known compound to date. ThO_2 can also be grown as a single crystal. It should be noted, however, that ThO_2 is not widely manufactured as demand is low and there are inherent safety concerns when dealing with Th as it is a radioactive substance.

Because yttria-stabilized zirconia (YSZ) is a material identified as alkali resistant, yttria itself may prove to be useful in resisting alkali-based damage and diffusion as well. Y_2O_3 is also a single crystal with decent transmission at the desired wavelength. It is for these reasons that this material will be tested. Specific physical properties of these materials are listed in Table 2.

Table 2. *Tabulated physical properties of crystalline oxides.*

MATERIAL	Structure	T_m [°C]	T_i [%] (at λ [nm])	ρ [g/cm^3]
BGO[18,19]	Cubic	1050	70 (500)	7.13
LYSO[18,20]	Monoclinic	2000	85 (600)	6.99
MgO[16]	Cubic	2800	84 (1000)	3.65
ThO_2[16,21]	Cubic	3050	76 (2500)	9.87
Y_2O_3[18,22]	Cubic	2410	60 (800)	5.01
ZrO_2[16,23]	Monoclinic	2700	80 (750)	5.82

3.2.3 Sapphire-like Materials

Sapphire has long been known to be a robust laser window material because of its mechanical strength, high optical transmission, high melting point, and ability to be grown as large single crystals. Sapphire is also a dense, highly crystalline material and has been suggested as a material that can resist alkali diffusion [7]. Sapphire itself will be tested, but since its alkali

resistance and physical properties are already known, two other sapphire-like materials were immediately selected to also be tested.

Aluminium oxynitride (ALON) is a transparent ceramic that is currently used in bullet- and blast-resistant windows. Its mechanical and thermal properties are nearly the same as sapphire. The inclusion of the nitride within the material may help to discourage alkali diffusion through the bulk material. It is transparent at 795 nm and because of its use as bullet- and blast-resistant windows is commercially available in relatively large amounts. Because it is a ceramic, however, it may not be as effective as single crystal materials for alkali resistance.

Another material that has similar qualities to sapphire is magnesium aluminate spinel. Spinel technically refers to a family of minerals with an octahedral structure with chemical composition of the form $A^{2+}B_2^{3+}O_4^{2-}$. As magnesium aluminate is the only member of the spinel family of materials that participated in this research effort, "spinel" shall refer only to magnesium aluminate $MgAl_2O_4$. Spinel is a hard, dense material that can be grown in single crystals. It has thermal, mechanical, and optical properties similar to sapphire and with the addition of Mg to the chemical structure, it may be more challenging for alkali metals to diffuse into the bulk as Mg is more similar to, for example Rb, than transition metals and may fill vacancies and defect sites that Rb might otherwise occupy and use to pull its way through the bulk material. Table 3 contains tabulated physical properties of sapphire-like materials.

Table 3. *Physical properties of sapphire and sapphire-like materials.*

MATERIAL	Structure	T_m [°C]	T_i [%] (at λ [nm])	ρ [g/cm^3]
Sapphire[16]	Hexagonal	2050	82 (1000)	3.99
ALON[24]	Polycrystalline	2150	85 (795)	3.70
Spinel[16]	Cubic	2135	90 (1000)	3.57

3.2.4 Rb-based Crystalline Materials

One working hypothesis regarding the diffusion of alkali metals is that they are finding and occupying vacancies within crystal lattices or are forcing out the native metal in the transparent material. If this is the case, a material that already has an alkali metal (e.g., Rb) incorporated into its lattice may discourage Rb for diffusing into the bulk, or at least mitigate the effect Rb has on bulk properties. $RbTiOAsO_4$ (rubidium titanyl arsenate or RTA) and $RbTiOPO_4$ (rubidium titanyl phosphate or RTP) are materials that incorporate Rb in their natural structure. Titanates, as was mentioned earlier, are also supposed to be resistant to alkali metals. RTA and RTP are also often advertised to have high damage thresholds [25]. Because of the combination of these materials, RTA and RTP may make for strong candidates for alkali resistant materials. Table 4 lists physical properties of RTA and RTP.

Table 4. *Physical properties of Rb-based glasses.*

MATERIAL	Structure	T_m [°C]	T_i [%] (at λ)	ρ [g/cm^3]
RTA	Orthorhombic [26]	1092 [27]	> 80 (visible) [28]	4.05 [29]
RTP	Orthorhombic [30]	1000 [31]	> 80 (visible) [28]	3.60 [25]

3.2.5 Perovskite Materials

Perovskite structured materials have a unique arrangement of atoms in the lattice; it is a variation of the cubic crystal structure. In general, perovskites have a chemical structure of ABO_3, where A and B are cations. The crystal structure is illustrated in Figure 4.

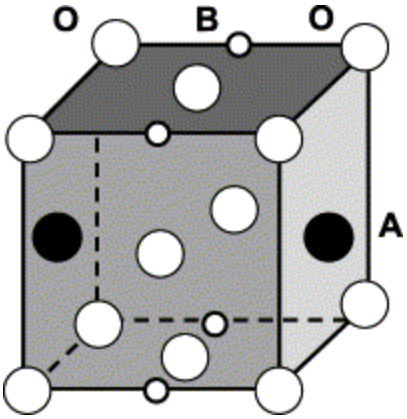

Figure 4. *Perovskite cubic cell structure. Adapted from [32].*

Some perovskite structured materials have been used for superconductivity, YBCO being a common example. Perovskites, such as $CdWO_4$, $KTaO_3$, and $LaAlO_3$, have been used as scintillators. The crystal structure is, in part, what lends to the special properties of perovskite materials. These three materials are of interest to this research because of their optical and mechanical properties and high density. They have a very dense crystal structure and have reasonable optical properties at 795 nm. Physical properties of perovskite structured materials are listed in Table 5.

Table 5. *Physical properties of perovskite structured materials.*

PEROVSKITE	Structure	T_m [°C]	T_i [%] (at λ [nm])	ρ [g/cm^3]
$CdWO_4$[18,33,34]	cubic	1271	75 (795)	7.90
$KTaO_3$[16,35]	cubic	1357	99 (900)	7.02
$LaAlO_3$[18,36,37]	cubic	2110	65 (750)	6.51
$SrTiO_3$[16]	cubic	1910	72 (1000)	5.11

3.2.6 Non-oxide Crystalline Materials

Because of alkali metals' propensity to migrate through an oxide network by bonding with oxygen, non-oxide materials may be advantageous. One such material that has been used as a laser

window is diamond. Carbon and alkali metals are not as likely to interact chemically. Additionally, because of the high thermal and mechanical strength, diamond may make a highly effective laser window. One factor to bear in mind, however, diamond's optical properties at 795 nm (T ~ 70 %, n ~ 2.4) may require additional finagling to improve transmission [38, 39]. Such work will be addressed briefly in Chapter 7.

Calcium fluoride is a dense, non-oxide cubic crystal with low refractive index and high optical transparency. CaF_2 is also a material that is already used in optics, both as a lens and windows and as an AR coating. Because fluorine is a principle part of CaF_2, there is some concern that an alkali metal-fluoride bond may be more favorable than the alkaline earth (Ca)-fluoride bond. This may accelerate alkali damage to CaF_2 as Ca-F bonds may be broken more aggressively than metal-oxide bonds. This material, however, may prove to be resilient and may provide insight on other candidate materials.

Table 6. *Physical properties of non-oxide crystals.*

MATERIAL	Structure	T_m [°C]	T_i [%] (at λ [nm])	ρ [g/cm^3]
CaF_2[16,18]	Cubic	1423	95 (1000)	3.18
Diamond[18,39]	Cubic	3730	70 (1000)	3.50

CHAPTER 4: ANALYSIS TECHNIQUES

Because of the experimental nature of this research, many techniques were used to characterize the candidate materials and to verify theories about the phenomenon being observed. The basic principles of each system, applications, and shortcomings will be discussed in this Chapter including an overview of the most important analysis methods. This will by no means be a comprehensive discussion of these systems, but enough information will be provided to ensure a working knowledge of them and an understanding of capabilities.

4.1 Spectrophotometry

Spectrophotometry is a technique that quantitatively measures the transmission of a material as a function of wavelength. This is done directly by passing light through the material and comparing how much light is passed through compared to how much light would reach the detector if there was no material. The specifics of operating spectrophotometers and some of their limitations are presented in 4.1.1.

4.1.1 Operating Principles of Spectrophotometry

Transmission is measured by direct comparison of the relative intensity of light passing through the sample material and the amount of light detected in the absence of such a sample. Figure 5 shows a typical setup for a spectrophotometer. In order to create a direct comparison of the intensity of the beam passing through a sample and in a sample's absence, the light source is usually split by a beam splitter. This creates two beams with the same intensity, one beam is passed directly to a detector and the other is passed to a second detector through the sample. The relative intensity from both beams is then compared to show the change in relative intensity. This change represents how much light from the medium reached the detector as compared to the reference. With this information, transmission can be determined.

Because a material's optical properties are wavelength-dependent, the light used must be monochromatic in order to give a representation of transmission at specific wavelengths. To accomplish this, multi-chromatic light sources are used and a diffraction grating separates the white light into (ideally) monochromatic rays which are used to determine transmission at specific wavelengths.

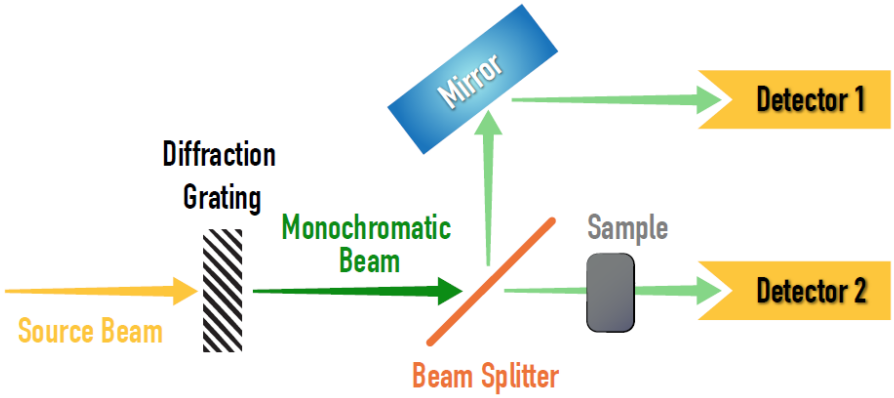

Figure 5. *A typical setup for a spectrophotometer.*

4.1.2 Using a Spectrophotometer

Spectrophotometers, while usually simple in operation, do require some amount of finesse when being used – specifically since calibration is important as is awareness of artifacts that can occur during a data acquisition cycle. Calibration methods vary from spectrophotometer to spectrophotometer, but the one used in this research effort required a zeroing-baseline calibrations. This is where the spectrophotometer will run through the spectrum of interest twice; the first time being where there is neither beam is obstructed. This creates a baseline of 100% transmission. The second run will involve the total obstruction of the probe beam resulting in a 0% transmission reference. After these two transmission curves are generated, the spectrophotometer will calibrate itself based on those curves.

Some spectrophotometers, like the one used in this research effort, will occasionally generate artifacts when collecting data. These artifacts arose due to either a change of light sources or diffraction gratings to assess transmission in different bands. So long as this is understood when taking data, it can be corrected either by fitting the spectrum or by retaking it.

4.2 Reflectometry

Reflectometry is a technique that can determine the reflectance of a material as a function of wavelength. Reflectance is measured directly by irradiating a sample with monochromatic light and measuring the intensity of light that is reflected from the surface of the sample and comparing it to the original intensity of the monochromatic light [40]. This gives a ratio of reflected intensity to incident intensity at a specific wavelength [40]. The specifics of how this is done are overviewed in 4.2.1.

4.2.1 Operating Principles of Reflectometry

The operating principles of reflectometry are fundamentally similar to spectrophotometry. A beam of light is split and part of the split beam is sent to a reference detector [40]. The second split beam is sent towards the sample which is placed in front of a diffuse absorptive backdrop. The backdrop prevents transmitted light from reflecting back through the sample and towards a second detector. This second detector measures the intensity of the light reflected off of the sample relative to the first split beam and from that reflectance is determined.

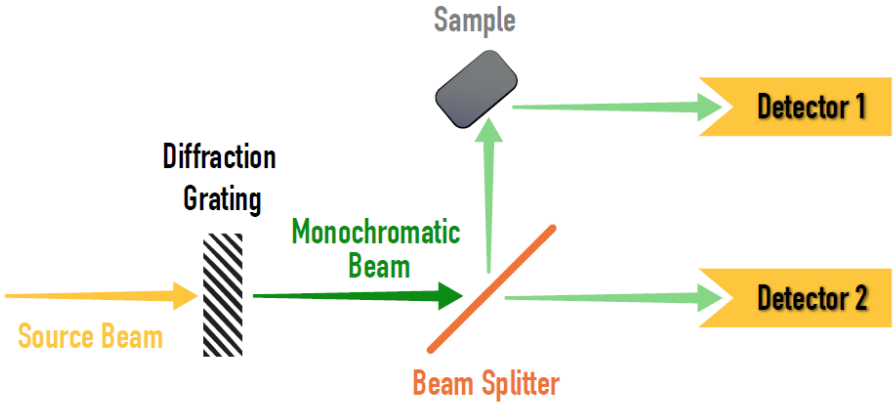

Figure 6. *An example of a reflectometer setup.*

4.2.2 Using a Reflectometer

In this research effort, reflectometry was conducted by attaching a differential reflectometer accessory to the spectrophotometer that was used to conduct transmission measurements. Much like when collecting transmission data, one had to calibrate the machine in order to obtain accurate reflection measurements. This is done through software calibrating itself to both 0% and 100% reflectance prior to analyzing a sample, just as with the spectrophotometer calibration.

4.3 X-ray Photoelectron Spectroscopy

X-ray photoelectron spectroscopy (XPS), also referred to as electron spectroscopy for chemical analysis (ESCA), is a surface analysis technique that can semi-quantitatively identify constituent elements of a material if the element is abundant enough – generally on the order of parts per thousand (ppt). Surface analysis generally refers to only with the first few atomic layers of a material, often between 0.1 nm and 10 nm. While XPS is not the most sensitive surface analysis technique, it is nonetheless used frequently in surface sciences. More details into operating mechanism and applications and limitations of XPS will be discussed in 4.3.1 and 4.3.2.

4.3.1 Operating Principles of XPS

The core mechanic behind XPS is the photoelectric effect. High powered X-rays bombard the surface of a material. These X-rays are capable of dislodging electrons from the material due to the interaction of electromagnetic radiation and the material (the photoelectric effect). These ejected photoelectrons move at a particular velocity away from the material. The velocity at which the photoelectron moves is directly related to the transformation of the energy carried by the X-ray ($h\nu$, where h is Planck's constant and ν is frequency) into the kinetic energy (E_K) of the photoelectron [41]. The amount of energy to generate a photoelectron is directly related to electron-nuclear interaction of the element, i.e. binding energy (E_B) of the photoelectron and the nucleus of the constituent atoms [41]. This relationship of energy is illustrated in Eq. (7)

$$E_B = h\nu - E_K \tag{7}$$

Additonally, the process by which XPS functions is illustrated in Figure 7.

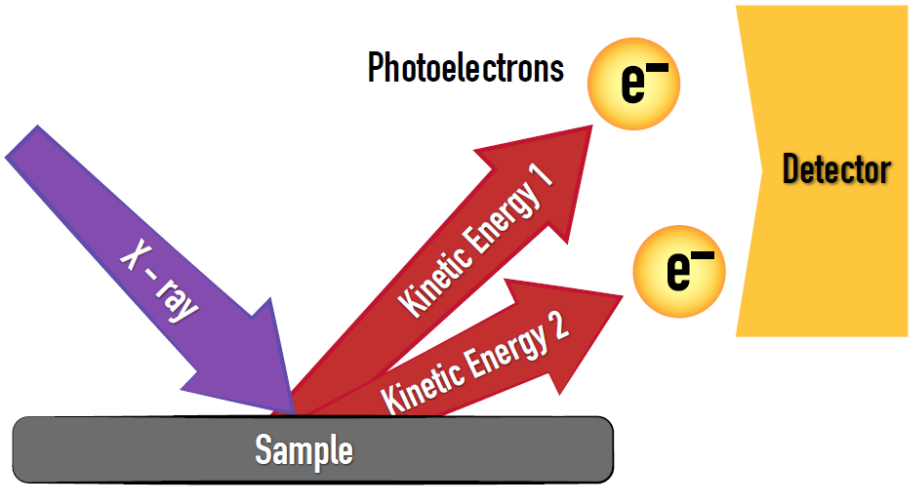

Figure 7. *A diagram of how XPS functions: the generation of photoelectrons with different kinetic energies from X-rays.*

Determining the binding energy is important because each element is defined by the number of protons in the nucleus, the amount of force (and therefore energy) that binds electrons

to the atom can serve as a signature of a particular element [41]. If the X-ray has that amount of energy equal to that state, then that is the amount of kinetic energy the photoelectron will be jettisoned with a specific velocity. The ejected photoelectron will then move into a magnetic field and will deflect the electron based on its speed. Based on the amount of deflection, an electron will strike a detector at a particular position. This position corresponds with a specific kinetic energy and therefore binding energy. With an ensemble of ejected particles, a spectrum of relative intensity vs. binding energy can be generated. This spectrum affords insight to the specific binding energies and therefore chemical composition of the sample being analyzed.

4.3.2 Limitation of XPS

While XPS is a versatile surface analysis technique, it does have limitations. The detection limit on many XPS systems is on the order of ppt. More sensitive surface techniques are required for more precise surface characterization, e.g., secondary ion mass spectroscopy. Because of the reliance of detecting photoelectrons, ultra-high vacuum conditions are often essential in order to both maximize the detected signal of the photoelectrons and to eliminate other particles from interacting with the detector. This often requires bulky vacuum chambers and expensive pumps. Additionally, because of the intrinsic nature of identifying elements based on electrical structure, XPS has difficulty identifying elements with an atomic number less than three since atoms like hydrogen, helium and lithium only have peaks in relatively low binding energies. This creates an issue in positively identifying these small atoms as nearly all other atoms also have peaks in the low energy regime.

4.4 Time of Flight Secondary Ion Mass Spectrometry

Time of flight secondary ion mass spectrometry (ToF-SIMS) is an extremely sensitive surface analysis technique that analyzes secondary ions from a sample by measuring how long

those ions take to move from the sample to the detector [42]. ToF-SIMS is capable of detecting concentrations of elements and molecules on the order of parts per billion (ppb) [42]. ToF-SIMS is, at its core, a mass spectroscopy technique that identifies atoms and molecules by their charge to mass ratio, from which atomic weight can be determined. The general operating principles and how they contrast from regular mass spectroscopy as well as applications and drawbacks of ToF-SIMS systems will be discussed in 4.4.1.

4.4.1 Operating Principles of ToF-SIMS

ToF-SIMS differs from regular mass spectroscopy in several ways. Instead of a sample being vaporized, an ion beam is used to bombard the surface of the solid sample, hereafter referred to as primary ions [42]. These primary ions can be liquid metal ions, Ga^+ or Cs^+, ionized noble gases, Ar^+ or Xe^+, oxygen ions, O^- or $O_2^{\pm}$, or other ions depending on the need and apparatus. The primary ions will ablate the surface of the sample generating ionized particles called secondary ions. The secondary ions will be either atoms of the constituent elements of the sample (these are emitted near incidence of the primary ion beam) or molecules that form the compound (these larger particles occur farther from where the primary ion beam strikes). The signed charge of the primary ions determines the charge of secondary ions emitted. The secondary ions are the analytes from which molecular weight can be determined and molecules identified.

The time of flight aspect of ToF-SIMS refers to the method by which the mass of analyte particles from the sample can be determined. The time of flight method is different from how ordinary mass spectrometers measure analyte particle mass. Because the ionized analytes have the same kinetic energy from the field it is possible to discriminate them based not only on their mass but also their velocity. In ToF-SIMS, the detectors can retrieve data about the charge-to-mass ratio based on how long the particles are “airborne,” i.e., how long they were in flight. It is important to

note that unlike regular mass spectrometers, ToF-SIMS cannot analyze a continuous stream of ions. The analyte ions must be sent through in pulses in order to accurately track their time of flight. This process is illustrated in Figure 8.

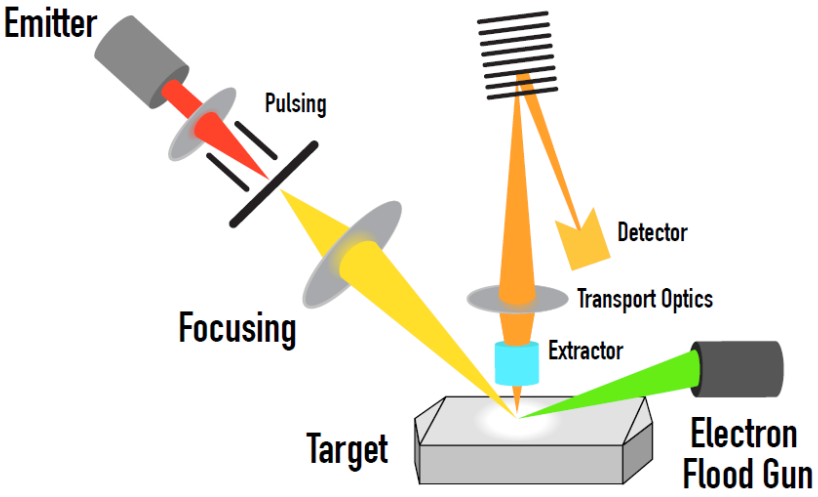

Figure 8. *A typical schematic of a ToF-SIMS system.*

ToF mass spectrometers have become more common for several reasons. ToF mass spectrometers have higher sensitivity and as such can detect particle concentrations on the order of 1 ppm or better [43]. Improved signal to noise ratio is often achieved because there are fewer ion-ion interactions while in flight owing to the fact that there are fewer particles in motion as the secondary ions are analyzed in pulses [43].

SIMS has several unique advantages over traditional mass spectroscopy systems. Solid samples can be analyzed easily since the primary ion source generates secondary ions from the sample, regardless of the phase of the sample. SIMS can provide highly localized surface analysis on samples. This is because the primary ion beam can be focused down to sub-micron sizes [42]. If secondary ions are only generated from sub-micron areas, then one can probe different places

on the same sample; this can be useful for identifying if the local chemistry is varying throughout a sample.

4.4.2 Applications and Limitation of ToF-SIMS

ToF-SIMS, while very useful in many respects, has its limitations. There are a number of drawbacks when using ToF-SIMS and these will be addressed. The disadvantages include: charge buildup on dielectric samples, ToF-SIMS cannot detect positive and negative secondary ions simultaneously, and sample damage [42, 44].

Charge buildup is not an uncommon problem when bombarding electrically insulating samples with charged particles. This charging, however, can be a detriment to analysis as built up charge can deflect primary ions from their intended target. This is usually corrected by a charge compensator – a low energy electron gun – that allows for the neutralization of surface charges thereby reducing surface charge effects.

As was discussed earlier, the signed charge of the primary ions used is an important aspect of ToF-SIMS analysis. A single polarity must be selected before beginning a ToF-SIMS analysis. Ions of opposite polarity than those being analyzed will not be detected in high enough quantities to perform the necessary analytics and information can be lost. Multiple analyses of the same sample using different polarity modes can achieve a more complete set of data, provided that the sample is intact enough for multiple analyses.

SIMS in general is a moderately destructive analysis technique. The expulsion of secondary ions from the surface unsurprisingly affects the topology of the sample. Continuous analysis on the same spot will cause more secondary ions to be emitted thereby making the damage worse. If the analyzed area has changed from its original state and only one polarity of ions was collected some information can be lost.

4.5 Ellipsometry

Ellipsometry is a technique that can be used to determine a number of physical features of a sample including composition, roughness, films thickness, crystallinity, and most commonly optical constants, specifically complex refractive index, $\tilde{n}$ [40]. While the full range of capabilities of ellipsometry is interesting and useful in many applications, this Section will focus exclusively on the determination of $\tilde{n}$. The complex refractive index, $\tilde{n}$ is defined to be $n + ik$ where n is the index of refraction and k is extinction coefficient (i is the imaginary unit). These values are found indirectly by measuring. This is done by measuring the complex reflectance ratio ρ in terms of intensity ψ and phase δ. In order to determine $\tilde{n}$, curve fitting of ψ and δ must be done and based on these curve fittings, refractive index and extinction coefficient can be calculated.

4.5.1 Operating Principles of Ellipsometry

Ellipsometry is based on Fresnel equations that govern how polarized light interacts with a sample [45]. The data collected from a sample does not directly yield the familiar optical or dielectric (tensor) values. Instead, the relative intensity and phase of the light are collected. The way how to find n and k will be discussed next, but for now the setup of the ellipsometer is reviewed. In general, a light source is passed through a polarizer in an effort to linearly polarize the electromagnetic radiation from the source. This now polarized source strikes the sample at some angle of incidence θ and is reflected off the surface. The reflected beam of light then passes through another polarizer and is then collected by a detector. This process is illustrated in Figure 9.

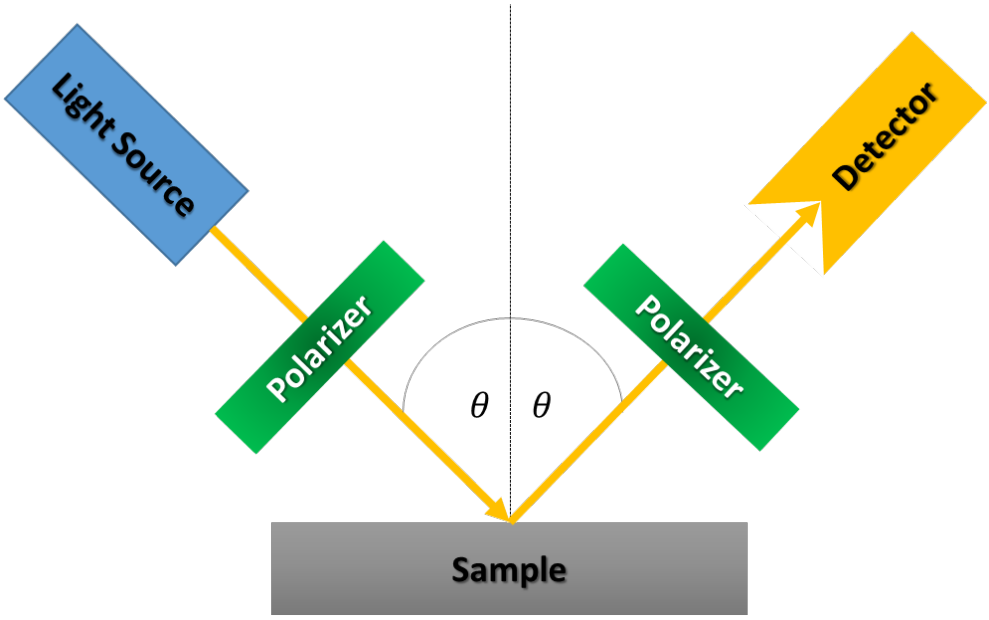

Figure 9. *A typical ellipsometer setup.*

This setup collects a piece of information known as the complex reflectance ratio ρ_R. This ratio is the quotient of the parallel and perpendicular reflectance coefficients r_p and r_s, respectively. This quotient can also be represented in terms of ψ and δ as shown in Eq. (8)

$$\rho_R = \tan\psi\, e^{i\delta} \tag{8}$$

with ψ and δ, complex refractive index $\tilde{n}$ can be calculated.

4.5.2 Determination of Complex Refractive Index

Finding n and k from ρ_R is not a trivial matter. A brief overview of a process by which n and k are determined will be presented herein; a more thorough explanation can be found in the papers published by Forouhi and Bloomer [46, 47]. A model of a dispersion relation must be generated in order to determine n and k. Forouhi and Bloomer derived dispersion equations for n (Eq. (9)) and k (Eq. (10)) as a function of wavelength λ. The case for amorphous materials will be shown here for the sake of simplicity; crystalline materials have similar dispersion relationships and similar logic applies to those equations and for other dispersion relations [46, 47]:

$$n(\lambda) = n_\infty + \frac{B_0(hc/\lambda)+C_0}{(hc/\lambda)^2-B(hc/\lambda)+C} \quad (9)$$

$$k(\lambda) = \frac{A((hc/\lambda)-E_g)^2}{(hc/\lambda)^2-B(hc/\lambda)+C} \quad (10)$$

where E_g is the bandgap energy of the material, h is Planck's constant, c is the speed of light in vacuum, A, B, and C are related to the broadening of bonding and antibonding states, $|\sigma_b\rangle$ and $|\sigma_a\rangle$ respectively, as shown in Eqs. (11) - (13) [46, 47]:

$$A = const.\times |\langle\sigma_a|\hat{x}|\sigma_b\rangle|^2\gamma \quad (11)$$

$$B = 2(E_a - E_b) \quad (12)$$

$$C = (E_a - E_b)^2 + \frac{(\gamma\hbar)^2}{4} \quad (13)$$

where γ is the inverse of the lifetime of the excited state to which the electron transfers, E_b and E_a are the energies associated with $|\sigma_b\rangle$ and $|\sigma_a\rangle$ respectively, and ħ is the reduced Planck's constant [46, 47]. Finally, B_0 and C_0 in Eq. (9) are related to A, B, and C in Eqs. (14) and (15) [46, 47]

$$B_0 = \frac{A}{Q}\left(\frac{-B^2}{2} + E_g - {E_g}^2 + C\right) \quad (14)$$

$$C_0 = \frac{A}{Q}\left(\left({E_g}^2 + C\right)\frac{B}{2} - 2E_gC\right) \quad (15)$$

where $Q = \frac{1}{2}\sqrt{4C - B^2}$. Solving for $n(\lambda)$ and $k(\lambda)$ is a difficult process that is often done by computation. Nonlinear least-squares curve fitting is often done to obtain A, B, C, and n_∞. Tauc-Lorentz, Cauchy, and Sellmeier are other dispersion models that can be used to obtain $n(\lambda)$ and $k(\lambda)$ [48, 49, 50].

4.6 Profilometry

Profilometry is a technique that is capable of providing surface morphology and roughness of a sample generally along a single line trace. The technique is relatively simple and height vs. position information is collected directly allowing for fast acquisition of topographic features of a

sample. From this, changes in height and roughness can be ascertained [51]. This information is often obtained by a fine tipped probe that is dragged across the surface of the sample being analyzed. As the probe is dragged, the relative height of the probe will change as a function of the surface morphology of the sample, i.e., if there are rises or indentations on the surface, the probe will have a different height than where it began when moving over those features [51]. These minute differences in height of the probe are often measured by piezoelectric or other mechanical configurations that are attached to the cantilever that the probe is attached to [51].

CHAPTER 5: EXPERIMENTAL

In an effort to improve the longevity of atomic physics based devices, an experimental research approach was developed in an effort to characterize candidate materials for their use in extreme alkali-rich environments. This Chapter will outline the research approach used to accomplish the goal of this project. The research was carried out as follows: (1) collect data on the physical (primarily optical) properties of the candidate material to serve as a baseline reference, (2) introduce the candidate materials to an environment that simulates conditions found in atomic clocks and DPAL systems, (3) the samples are then re-characterized to identify changes in physical properties, (4) finally, the samples are analyzed by ToF-SIMS in order to ascertain the extent of alkali diffusion into the bulk material.

5.1 Baseline Characterization

All materials underwent analysis to determine their ordinary optical and structural properties. Techniques used included spectrophotometry, reflectometry, and ellipsometry measurements. Spectrophotometry was done with a Cary 5000 UV-vis-IR spectrometer. As was mentioned earlier, reflectometry was done by installing a differential reflectometer accessory to the Cary 5000. Ellipsometry was done using a Bruker ellipsometer. The most vital baseline characterization was spectrophotometry and reflectometry in order to ascertain the sample's base transmittance and reflectance. Most transmission and reflectance values were collected between 200 nm and 1000 nm in order to have available a full transmission spectrum in case any future applications required a wavelength that was different than the 318-795 nm range. This data is later compared to the same kind of characterization after the samples have been exposed to Rb in the simulated environment that was constructed as an alkali diffusion testbed.

5.2 Simulated Environment

A small cell was constructed in an effort to simulate the extreme environments akin to those in atomic clocks and DPAL laser cavities. This cell is shown in Figure 10. It was made out of 316H stainless steel with Ag-coated Cu gaskets for the conflat flange connections, the cell has two major chambers – the sample storage area and the alkali source. As their names imply, the sample storage area is where candidate materials are kept during alkali exposure and the alkali source houses the alkali. Both areas could be heated independently with heater tape, each controlled by a variac (variable power supply). Heater tape was used to create a temperature gradient between the alkali and the samples in order to encourage diffusion of alkali metal vapor from alkali Rb source to the sample storage. Diffusion was affected by keeping the alkali source at higher temperatures than the sample storage area. Typical temperature gradients were generated by a ~ 100 °C difference in temperature, but a few other experiments were conducted using other temperature differences (these will be discussed in more details in Chapters 6 and 7). All reactions involving candidate materials were conducted with the alkali source cell at ~ 550 °C and the sample cell at ~ 450 °C.

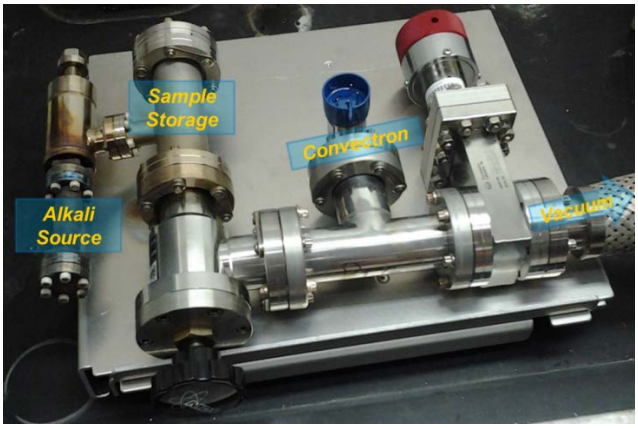

Figure 10. *Alkali exposure cell. The alkali source and sample storage areas are heated with heater tape and can be heated independently to create a thermal gradient.*

Once samples and alkali were loaded into the chamber, it was pumped to rough vacuum (~ 50 mTorr) using an Agilent SH-110 dry scroll pump. This was done to minimize the reaction of the alkali metal with atmospheric gases, particularly water. The pressure of the cell could be measured via a convection, however while the alkali was vaporous the convectron was never used as there was a concern that the alkali might damage the convectron. Once the alkali vaporized, 1 g of Rb in the case of the research presented here, there was an estimated 1 atm of pressure within the cell.

Samples were generally left in the alkali exposure cell for one week at a time. Other exposure durations were used in part to determine a diffusion trend. This trend was determined by a fused silica substrate that was included in most reactions in order to compare the diffusion that occurred in one reaction with another. These substrates also served as a kind of control to assess how each reaction performed compared to other reactions.

5.3 Recharacterization

After the candidate materials were exposed to a high temperature alkali-rich environment, the same battery of analysis conducted prior to exposure was repeated. This allowed for a direct comparison of the optical properties before and after the samples when they were placed in the simulated environment in an effort to determine how the diffusion of Rb affected transmission, reflection, etc. The differences in optical properties are summarized in Table 7 in Chapter 6.

5.4 ToF-SIMS Analysis

ToF-SIMS was instrumental in this research effort. An IonToF ToF-SIMS system was used to conduct all ToF-SIMS analyses. After each sample was exposed to Rb vapor at high temperatures, a ToF-SIMS depth profile was conducted to determine the extent of the Rb diffusion. The ToF-SIMS was used a Bi emitter and an O_2 sputter gun. The bismuth emitter was maintained

at 1 μA throughout the run and the oxygen sputtering was held at 2 kV. One or two spots were analyzed on each sample. Samples underwent cycles of sputtering using the O_2^- ions for 45 s and then the newly exposed surface was analyzed for 20 s and analysis was conducted 1,000 times, or until a "zero" point of Rb was reached. This "zero" point will be discussed later in 6.3.

The diffusion depth, z_d, of the various samples are summarized in Table 7 in Chapter 6. Diffusion depth, however is, is not intrinsically given in the ToF-SIMS that was used. Diffusion depth is calculated by taking the total physical depth bored into the sample and dividing that value by the length of time spent sputtering. The sputter time is recorded in the ToF-SIMS control software and the depth bored was found via Bruker Dektak XT profilometer. With both of these pieces of information, the physical depth of the diffusion of Rb can be ascertained.

CHAPTER 6: RESULTS

This Chapter will present the data collected on the candidate materials that were used in this research. A list of materials characterized and the results of those characterizations will be presented herein. The materials that were of great interest were ZrO_2, ALON, spinel, $LaAlO_3$, $CdWO_4$, and $KTaO_3$ (an explanation of why they are of interest will be given and a more in depth discussion and analysis of the data collected will be presented in Chapter 7).

6.1 Optical Characterization

Transmission T and reflection R of the samples studied were collected. Initial transmission and changes in transmission and reflection are tabulated in Table 7 in 6.3. It should be noted that changes in absorption R listed in Table 7 were not measured directly. Instead, it was calculated by the simple relationship between reflection, absorption, and transmission: $R + A + T = 1$ since R and T were measured. The following Sections will contain transmission and reflectance data of all

samples studied. Some complex refractive data is also presented, but elliposmetric data was not collected for all samples due to difficulties in fitting ψ and δ curves.

6.1.1 Amorphous Materials

Amorphous materials' optical properties were measured before and after exposure to Rb. In general, the transmission of the samples decreased slightly after exposure to Rb. The spectra collected for fused silica, Schott 8436 glass, and TAFD-40 are shown in Figures 11-13.

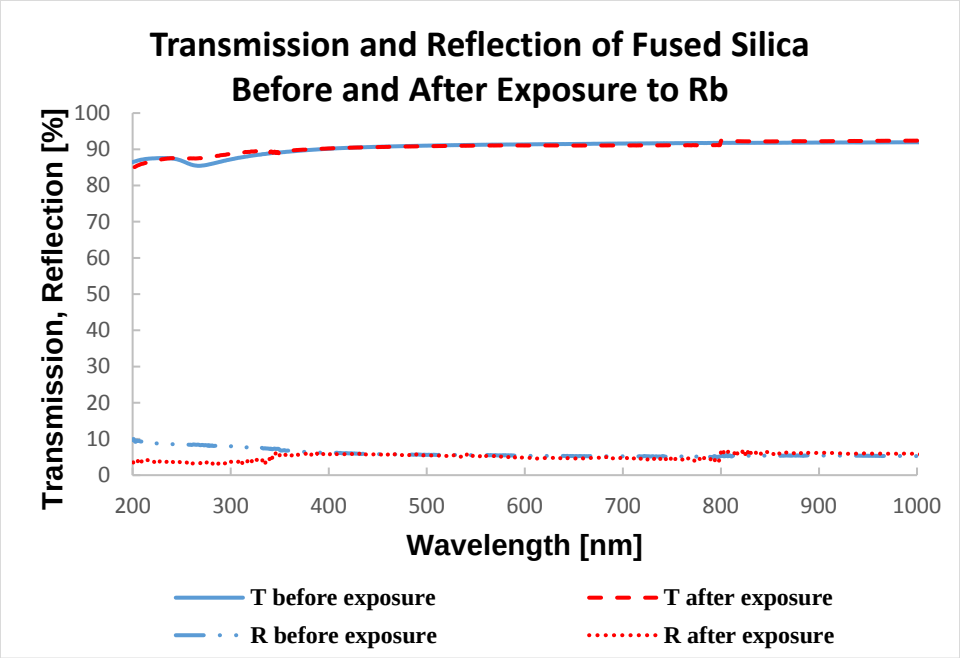

Figure 11. *Comparison of transmission pre- (solid blue) and post-exposure (dashed red) and of reflection pre- (dotted and dashed blue) and post-exposure (dotted red) of fused silica as a function of wavelength.*

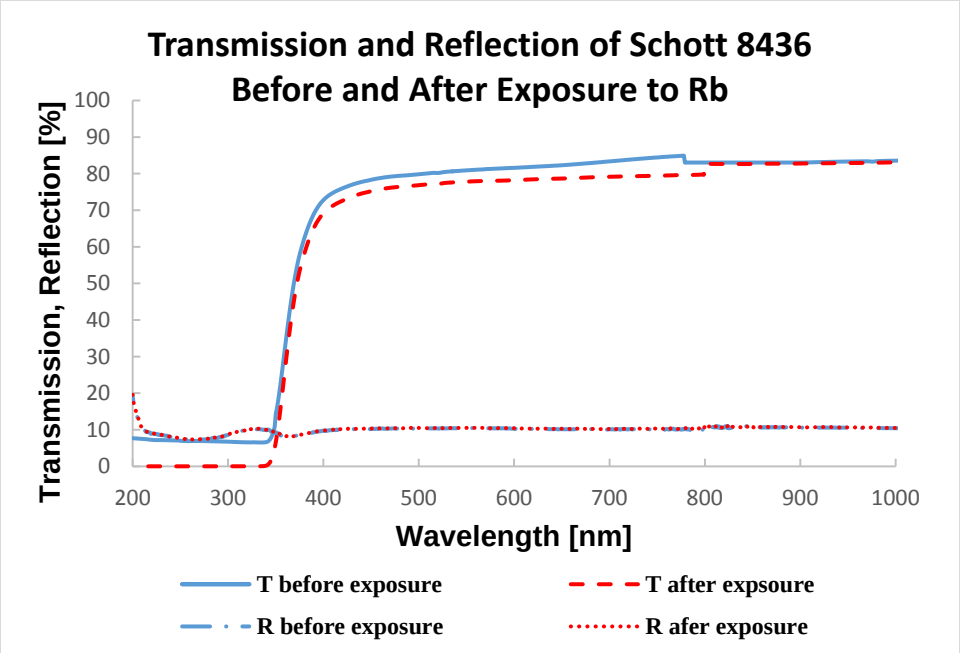

Figure 12. *Comparison of transmission pre- (solid blue) and post-exposure (dashed red) and of reflection pre- (dotted and dashed blue) and post-exposure (dotted red) of Schott 8436 glass as a function of wavelength.*

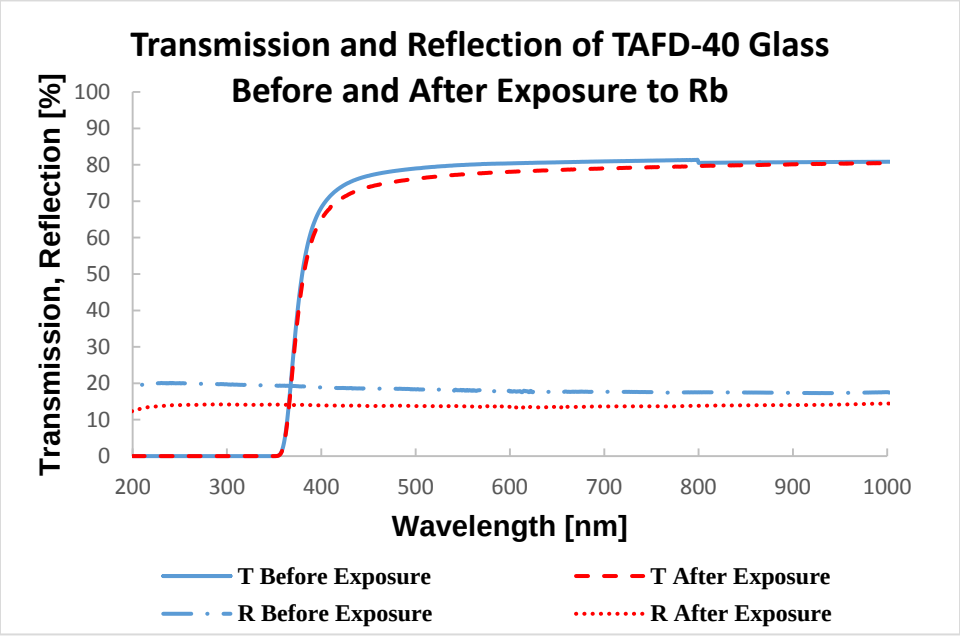

Figure 13. *Comparison of transmission pre- (solid blue) and post-exposure (dashed red) and of reflection pre- (dotted and dashed blue) and post-exposure (dotted red) of TAFD-40 as a function of wavelength.*

6.1.2 Crystalline Oxides

Optical properties of crystalline oxides were measured before and after exposure to Rb. Overall, exposure to Rb and high temperatures resulted in minor decreases in transmission. The spectra collected for cubic zirconia, LYSO, MgO, and Y_2O_3 are shown in Figures 15-18. BGO was destroyed in the reaction vessel in the process of being exposed to high temperatures and Rb vapor for one week. It appeared that a chemical reaction occurred and the BGO sample became dark and opaque (as shown in Figure 14) and became extremely fragile.

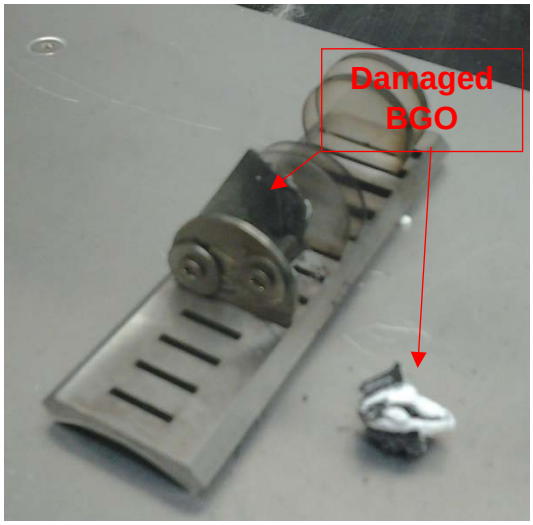

Figure 14. *BGO after being exposed to Rb for one week in the reaction vessel. Note the white "growth" occurring on the material and its opacity.*

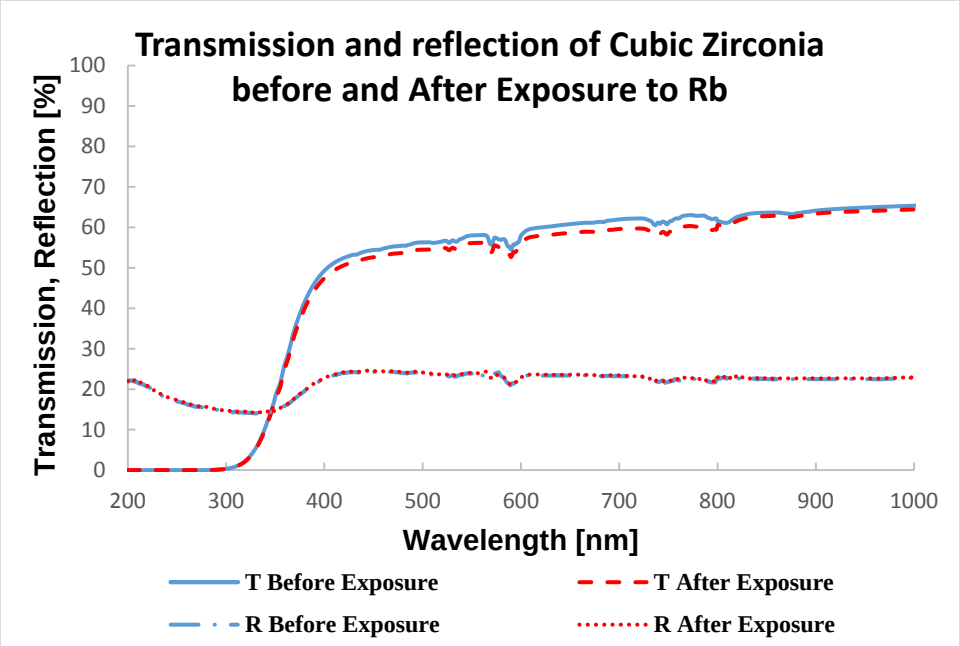

Figure 15. *Comparison of transmission pre- (solid blue) and post-exposure (dashed red) and of reflection pre- (dotted and dashed blue) and post-exposure (dotted red) of ZrO_2 glass as a function of wavelength.*

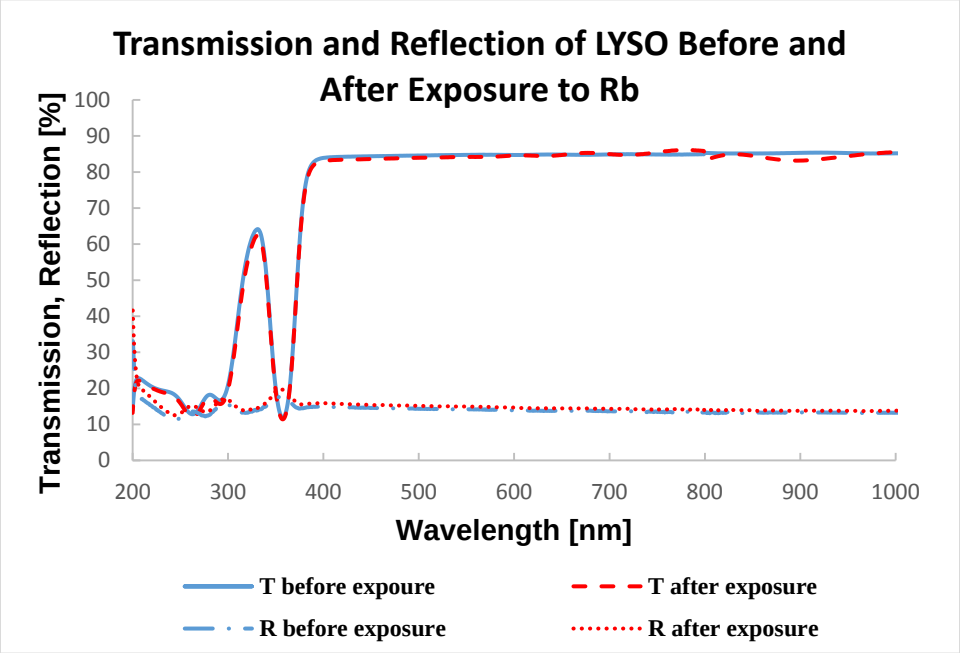

Figure 16. *Comparison of transmission pre- (solid blue) and post-exposure (dashed red) and of reflection pre- (dotted and dashed blue) and post-exposure (dotted red) of LYSO as a function of wavelength.*

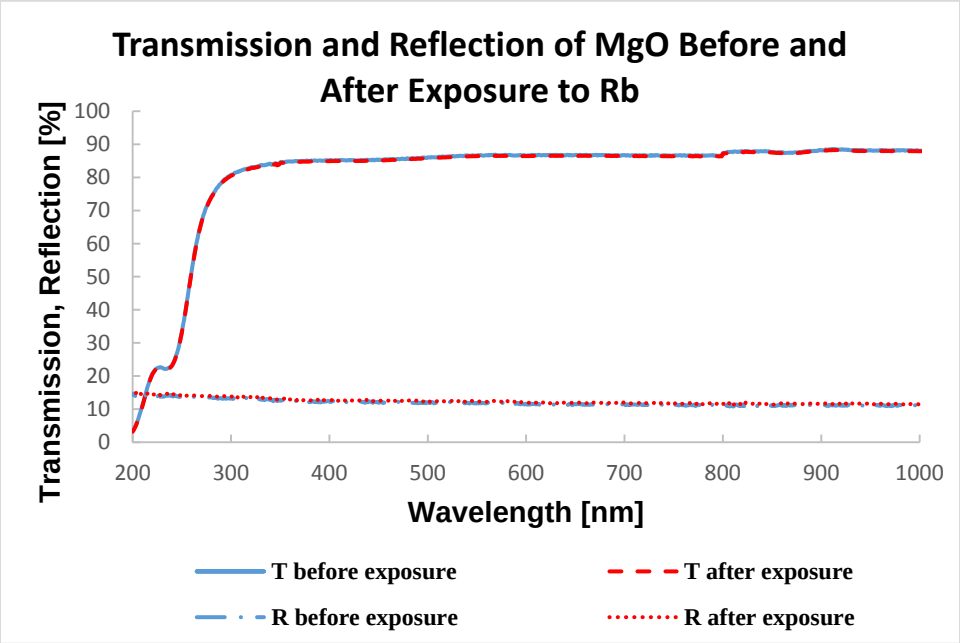

Figure 17. *Comparison of transmission pre- (solid blue) and post-exposure (dashed red) and of reflection pre- (dotted and dashed blue) and post-exposure (dotted red) of MgO as a function of wavelength.*

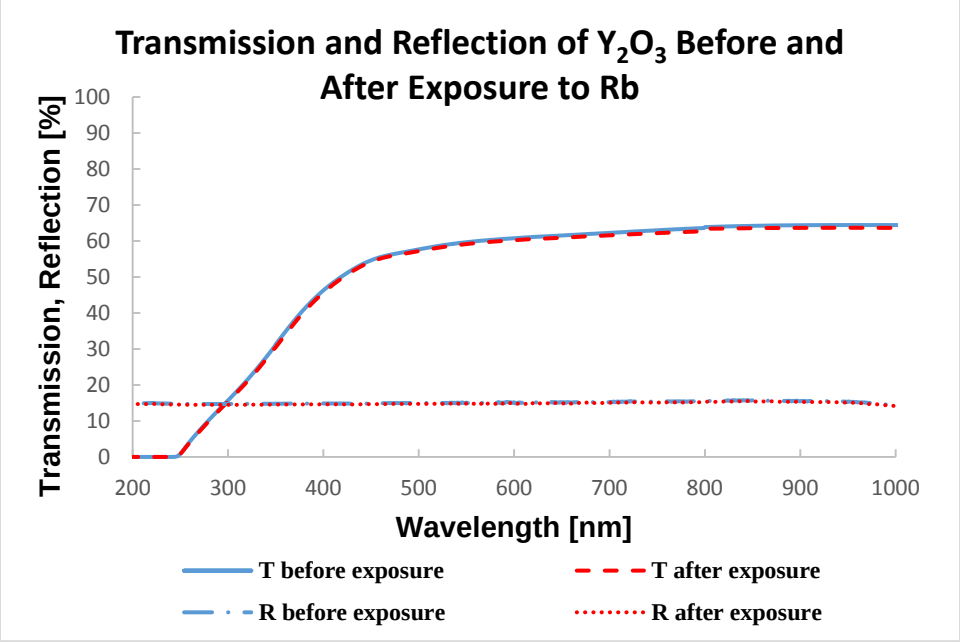

Figure 18. *Comparison of transmission pre- (solid blue) and post-exposure (dashed red) and of reflection pre- (dotted and dashed blue) and post-exposure (dotted red) Y_2O_3 as a function of wavelength.*

6.1.3 Sapphire-like Materials

Optical properties of sapphire-like materials were measured before and after exposure to Rb. The changes in optical properties were largely small decreases in transmission. The spectra collected for sapphire, spinel, and ALON are shown in Figures 19-21.

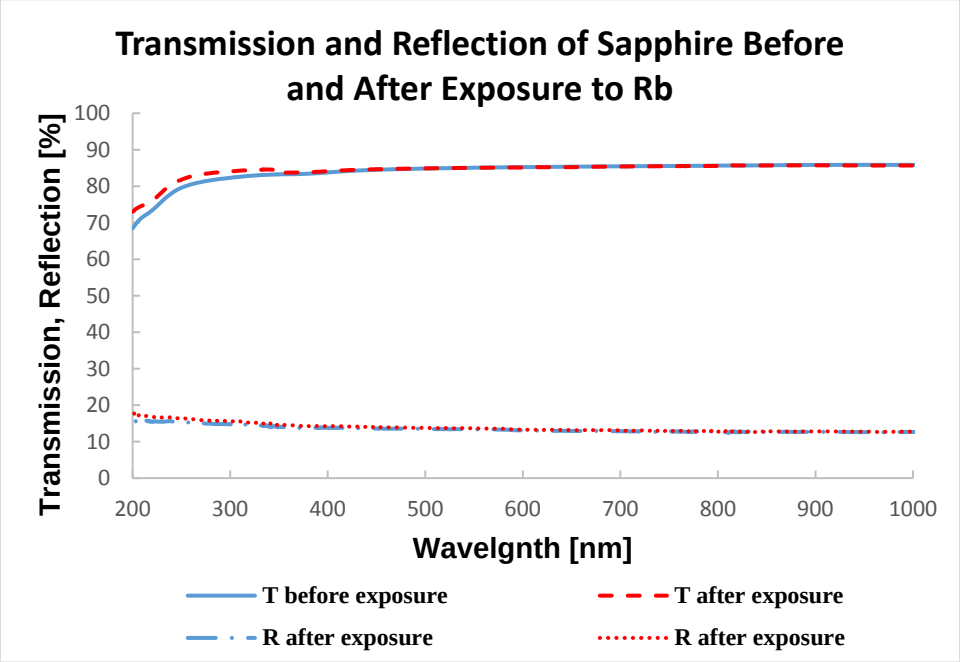

Figure 19. *Comparison of transmission pre- (solid blue) and post-exposure (dashed red) and of reflection pre- (dotted and dashed blue) and post-exposure (dotted red) of sapphire as a function of wavelength.*

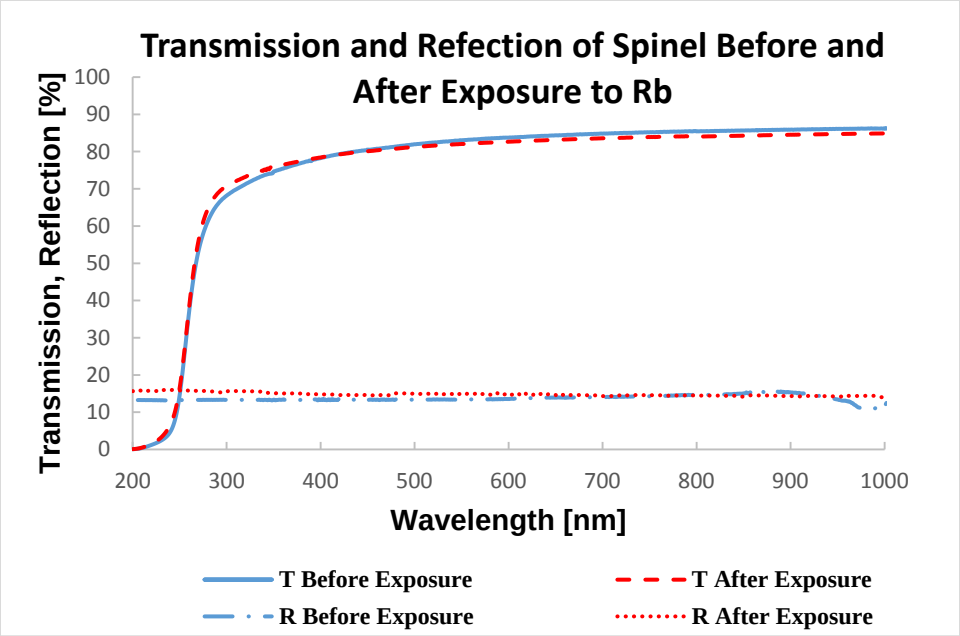

Figure 20. *Comparison of transmission pre- (solid blue) and post-exposure (dashed red) and of reflection pre- (dotted and dashed blue) and post-exposure (dotted red) of spinel as a function of wavelength.*

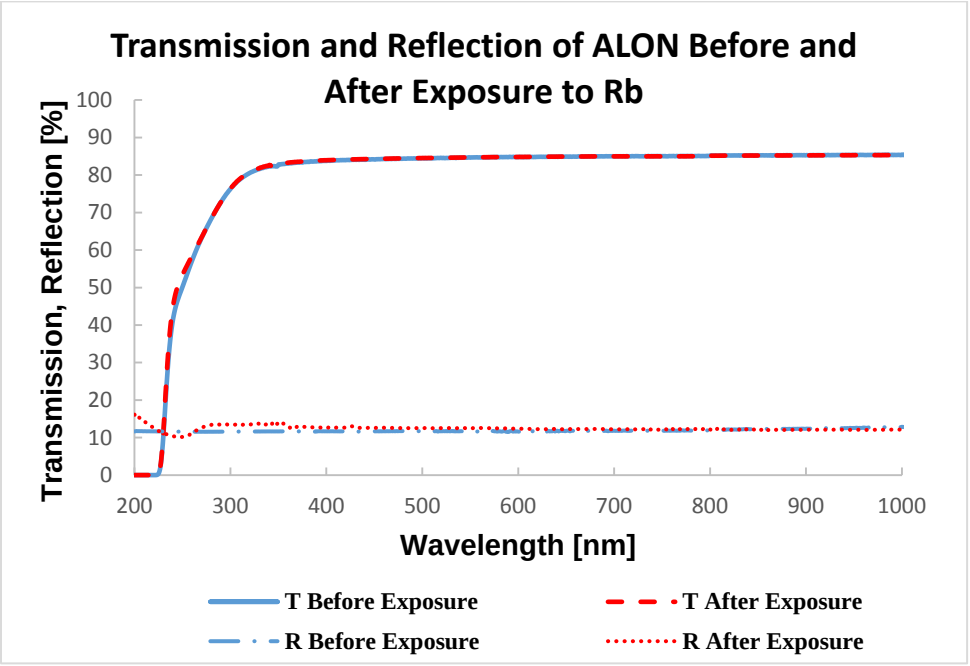

Figure 21. *Comparison of ALON's transmission pre- (solid blue) and post-exposure (dashed red) and of reflection pre- (dotted and dashed blue) and post-exposure (dotted red) as a function of wavelength.*

6.1.4 Rb-based Crystalline Materials

Optical data for Rb-based crystalline materials was collected. Both RTA and RTP were destroyed in the reaction. It is unclear as to why this occurred. There was one difference of note in the exposure they were involved in: carbon foam was also present in the reactor. This carbon foam disintegrated during this reaction and covered the interior of the reaction vessel and all samples therein. Figure 22 illustrates the state of the samples after the reaction.

6.1.5 Perovskite Materials

Perovskite materials exhibited unusual changes in optical properties after exposure to Rb. Figures 23−26 illustrate the increase in transmission of $LaAlO_3$, $CdWO_4$, $KTaO_3$, and $SrTiO_3$. A brief discussion of this phenomenon will be presented in Chapter 7.

Figure 22. *Image of the result of RTA and RTP after exposure to Rb at high temperatures.*

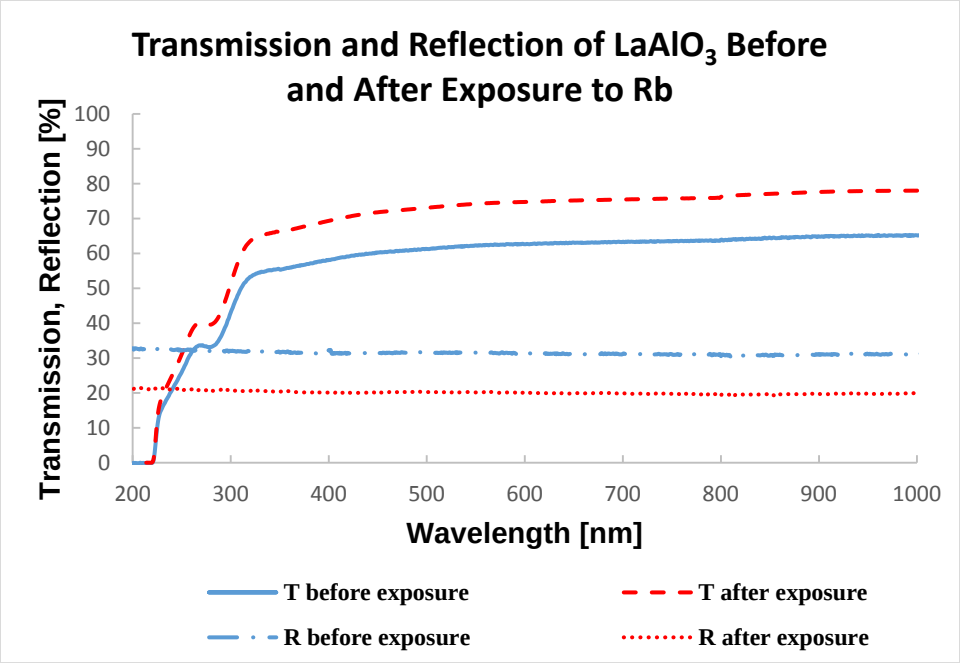

Figure 23. *Comparison of $LaAlO_3$'s transmission pre- (solid blue) and post-exposure (dashed red) and of reflection pre- (dotted and dashed blue) and post-exposure (dotted red) as a function of wavelength.*

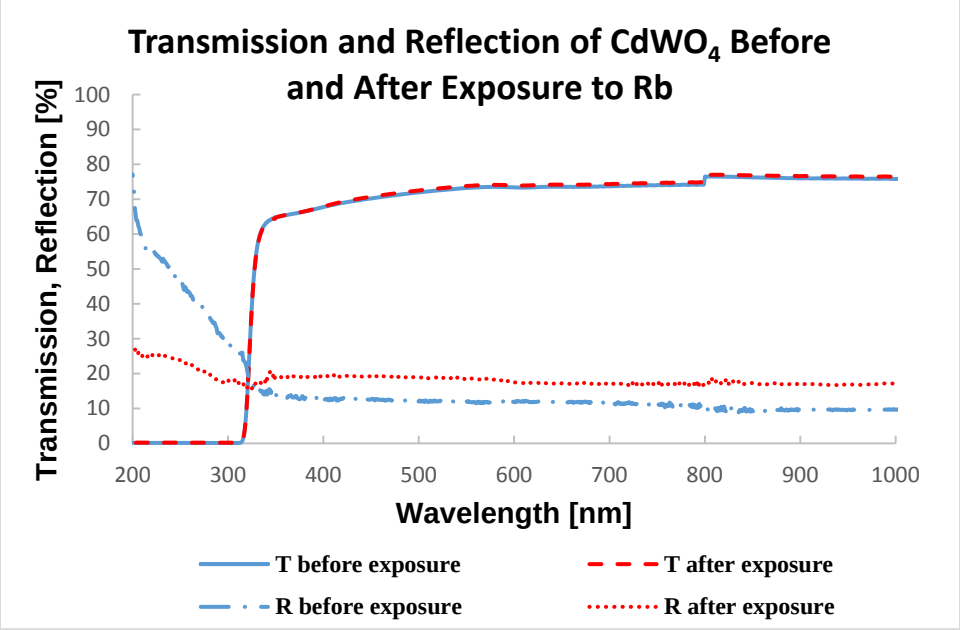

Figure 24. *Comparison of transmission pre- (solid blue) and post-exposure (dashed red) and of reflection pre- (dotted and dashed blue) and post-exposure (dotted red) of $CdWO_4$ as a function of wavelength.*

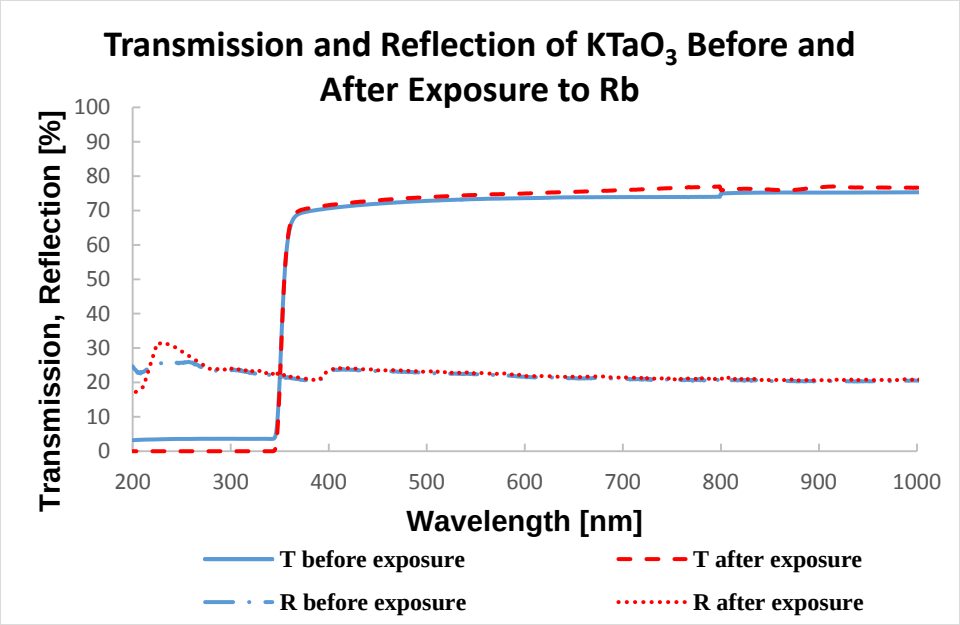

Figure 25. *Comparison of transmission pre- (solid blue) and post-exposure (dashed red) and of reflection pre- (dotted and dashed blue) and post-exposure (dotted red) of $KTaO_3$ as a function of wavelength.*

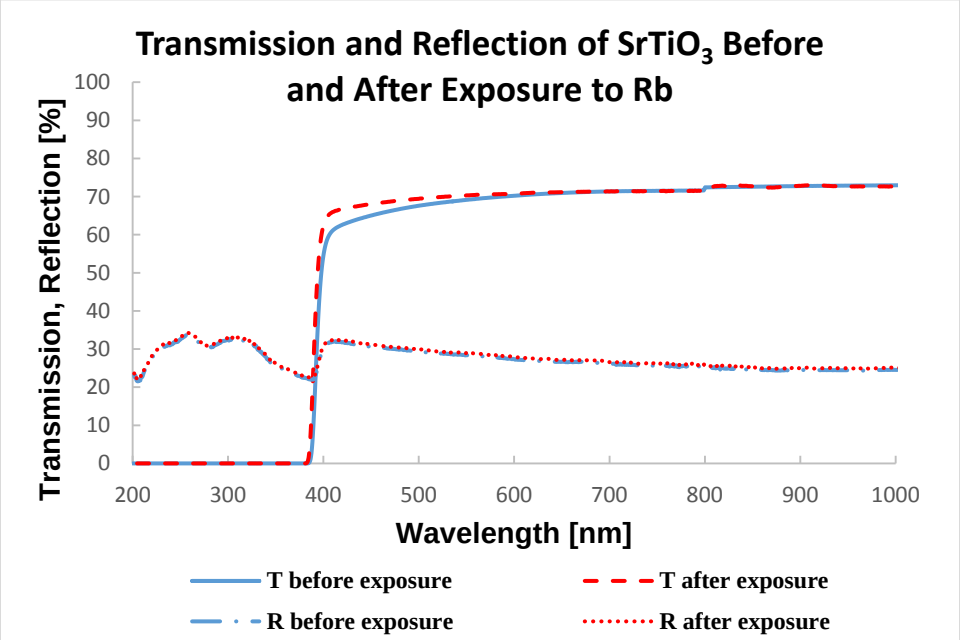

Figure 26. *Comparison of transmission pre- (solid blue) and post-exposure (dashed red) and of reflection pre- (dotted and dashed blue) and post-exposure (dotted red) of $SrTiO_3$ as a function of wavelength.*

Further investigation of the anomalous behavior of the perovskite structured materials involved an ellipsometric analysis of $LaAlO_3$, as shown in Figure 27. It should be noted that the

refractive index decreased while the extinction coefficient increased. This is consistent with the transmission and reflection data which indicates that there was no error in the spectrophotometric data.

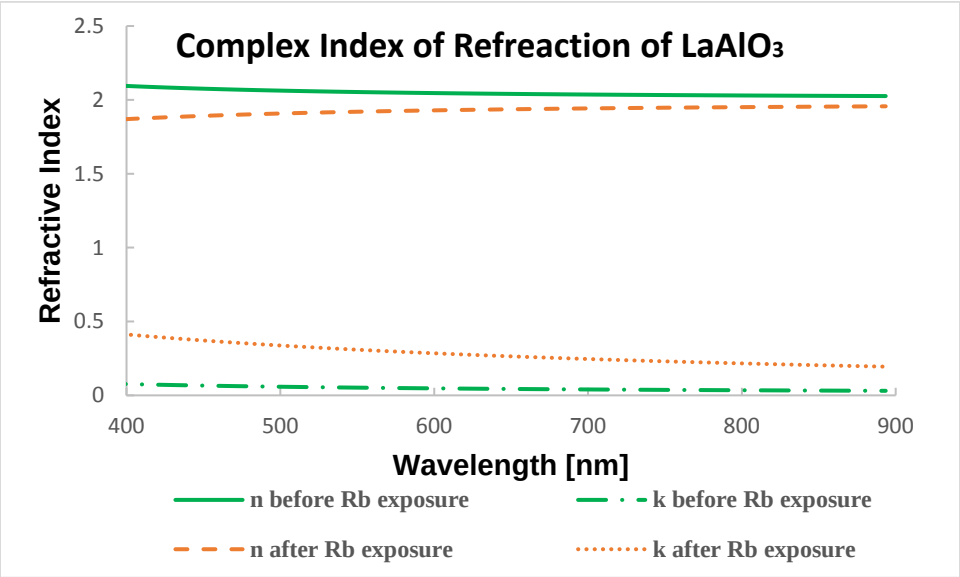

Figure 27. *Refractive index before (solid green) and after (dashed orange) exposure to Rb as well as extinction coefficient before (dashed and dotted green) and after (dotted orange) exposure to Rb of $LaAlO_3$ as a function of wavelength.*

6.1.6 Non-oxide Crystalline Materials

Transmission and reflection data was collected on the non-oxide crystals, CaF_2 and diamond. CaF_2's transmission decreased greatly after exposure while diamond's transmission was largely unchanged. This is illustrated in Figures 28 and 29.

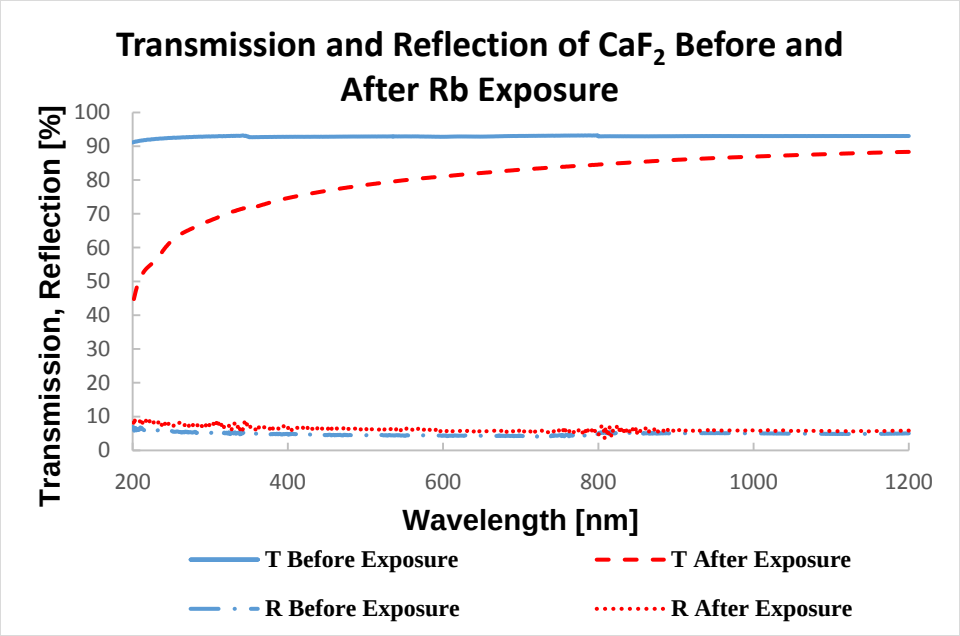

Figure 28. *Comparison of transmission pre- (solid blue) and post-exposure (dashed red) and of reflection pre- (dotted and dashed blue) and post-exposure (dotted red) of CaF_2 as a function of wavelength.*

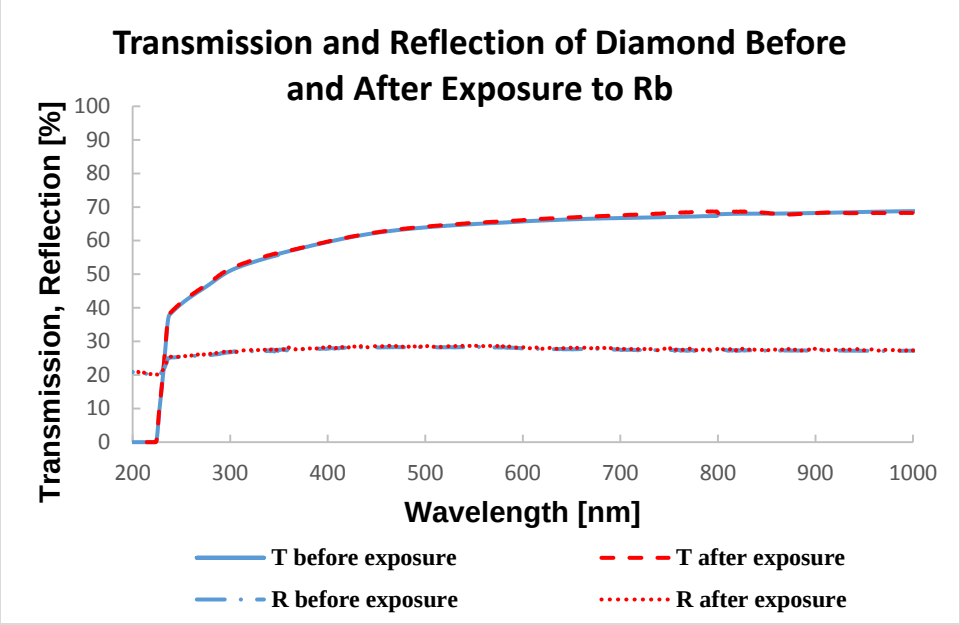

Figure 29. *Comparison of transmission pre- (solid blue) and post-exposure (dashed red) and of reflection pre- (dotted and dashed blue) and post-exposure (dotted red) of diamond as a function of wavelength.*

6.2 Diffusion Study

As was discussed in Chapter 5, ToF-SIMS was to analyze the extent of the Rb diffusion within the candidate materials. Several exemplary ToF-SIMS depth profiles are shown below such as in Figure 30. It can be seen from Figure 30 that the Rb diffuses into the material showing relative abundance as a function of sputter time – sputter time is related to the depth of penetration of the sample through the sputter rate. It is important to note the point at which a stoppage in diffusion was declared. When the relative abundance of Rb was on the order of several tens after successive data samplings, diffusion was said to have ended.

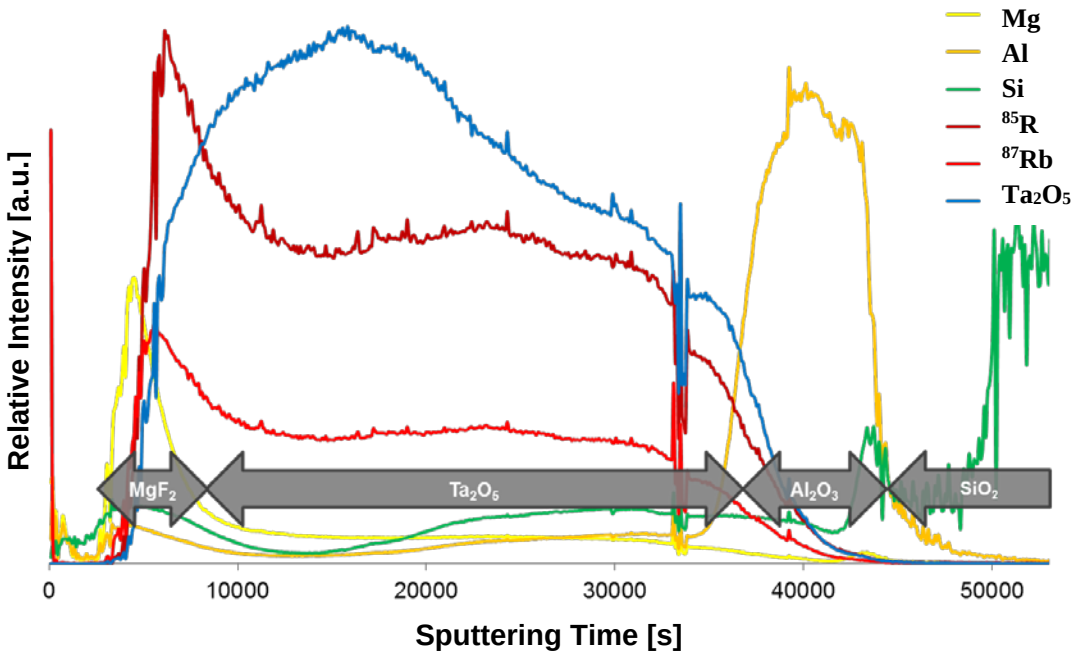

Figure 30. *A ToF-SIMS depth profile of a used DPAL window showing the extent of the Rb diffusion. The sputter rate allows the diffusion depth to be on the order of 3 µm.*

XPS analysis was conducted in order to confirm the results of ToF-SIMS. Figure 31 shows an XPS depth profile on the same DPAL window as shown in Figure 30. The XPS spectra identify the same constituent elements that were detected by ToF-SIMS on each layer of the AR coating.

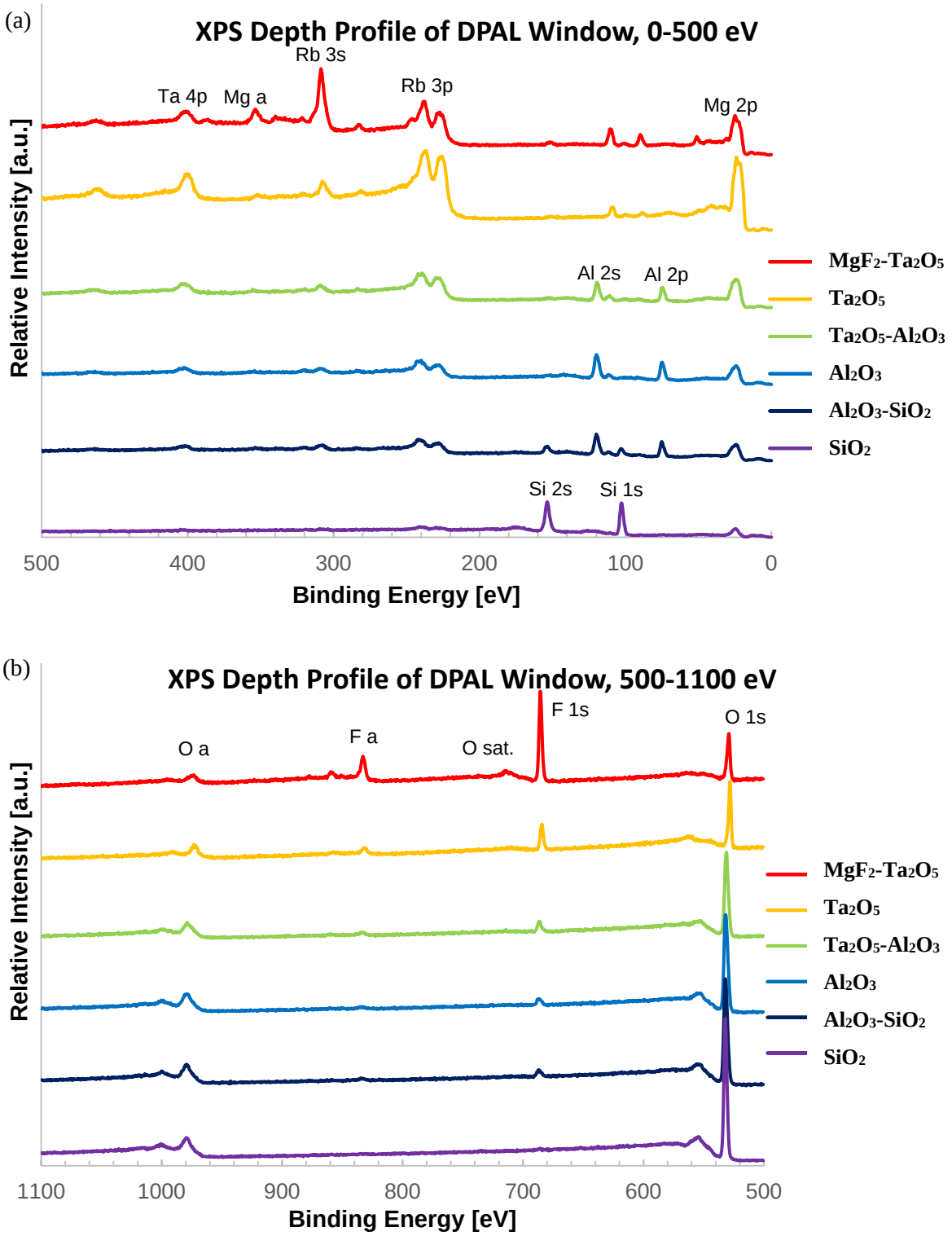

Figure 31. *Successive XPS spectra done on a DPAL window to confirm ToF-SIMS data. The different spectra coorispond to the layers of the AR coating on the wondow.These layers were reached by sputtering the surface of the sample with an ion gun. Spectra between 0 and 500 eV and between 500 eV and 1100 eV are shown in (a) and (b), respectively. Peaks of interest have been labeled.*

An interesting observation was made when analyzing the exposed and damaged DPAL windows. Because the DPAL windows had AR coatings on the surface, ToF-SIMS showed that the Rb "dragged" F from the MgF_2 coating deeper into the window – that is to say that F was found beyond the point of where the MgF_2 coating was. Additionally, ToF-SIMS showed that the F seemed to build up at interfaces between the other AR coatings. This phenomenon is shown in Figure 32. While this is not directly significant to the materials study aspect of this research, it is something to note when discussing a solution to the issue of creating effective DPAL windows.

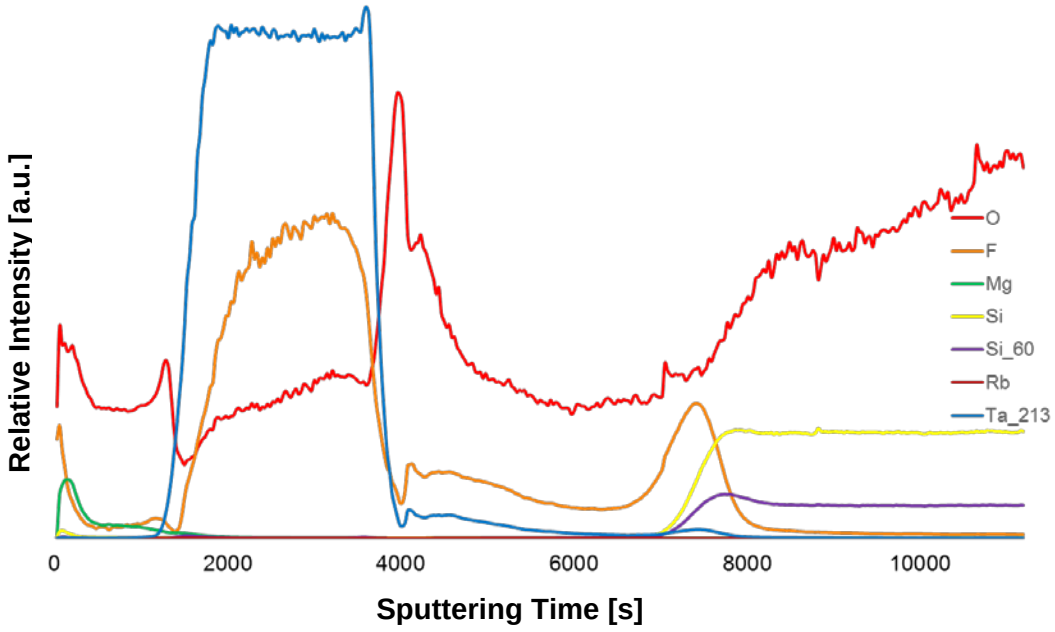

Figure 32. *A ToF-SISM depth profile of a DPAL window showing that as the Rb (red) diffuses through the material, F (orange) is carried into the bulk.*

Several other exemplary ToF-SIMS depth profiles are presented in Figures 33 and 34. It should be noted that Rb was said to have stopped diffusing if its relative intensity reached 50 counts.

6.3 Tabulated Results

The results of optical characterization and ToF-SIMS depth profiling are summarized

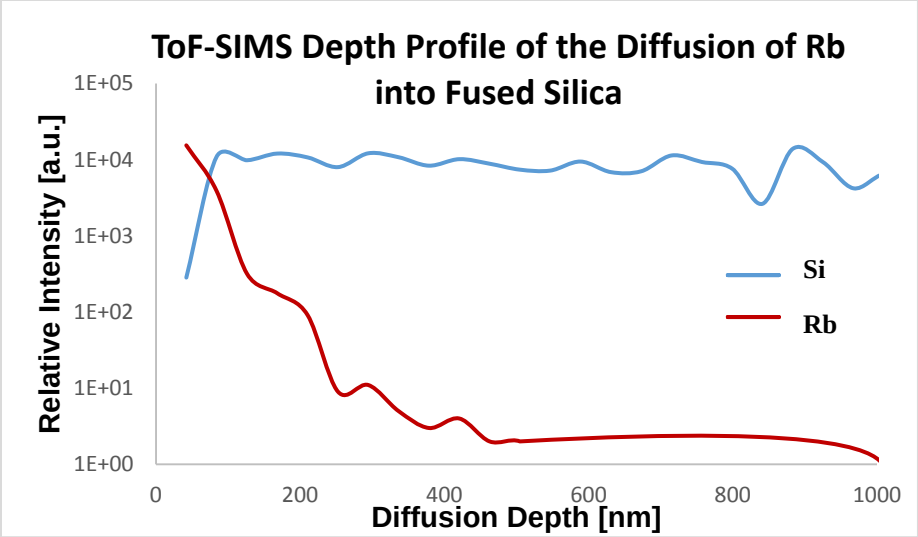

Figure 33. *ToF-SIMS depth profile of fused silica after exposure to Rb.*

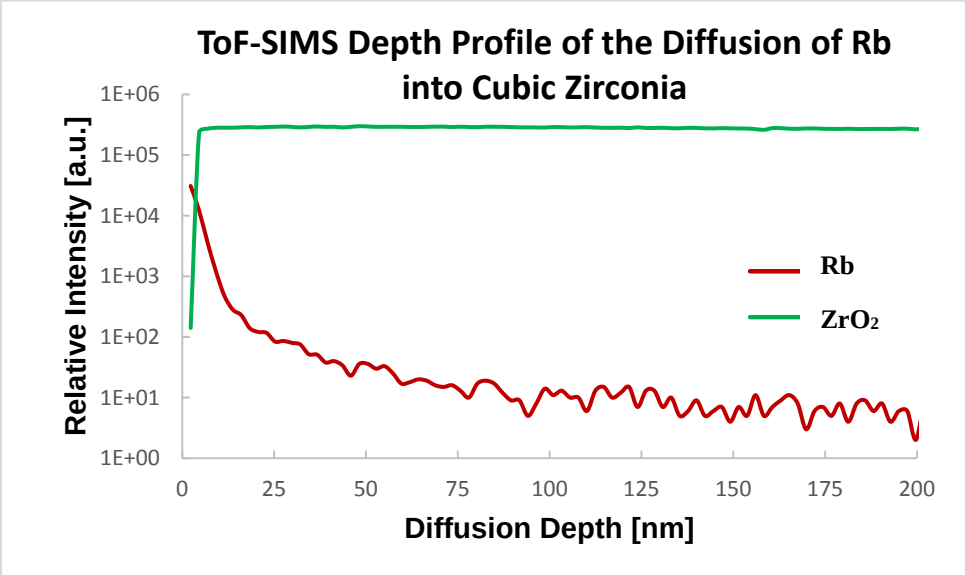

Figure 34. *ToS-SIMS depth profile of cubic zirconia after exposure to Rb.*

in Table 7. Several things to note regarding the data presented in Table 7 are that diffusion depth z_d was recorded using the experimentally obtained sputter rate as was discussed in 5.4 and that diffusion was assumed to end when counts of Rb was on the order of several ten for after successive analysis iterations. Information from this table will be discussed extensively in Chapter 7.

Table 7. *A list of materials studied. ΔR, ΔA, and ΔT are the relative changes in reflection, absorption, and transmission respectively at 795 nm from before and after the samples were exposed in the Rb exposure testbed. A*

positive number indicates an increase in an optical property relative to the sample before exposure and a negative number indicates a decrease. T_i is the initial transmission of the material to give reference to its inherent ability to transmit at 795 nm. The diffusion depth, z_d, is a statement of how deep the Rb diffused into the sample.

MATERIAL	T_i[%]	ΔR[%]	ΔA[%]	ΔT[%]	z_d[nm]
ALON	84.78	-1.78	+1.47	+0.31	55
BGO	77.95	SAMPLE DESTROYED IN REACTION			
CaF_2	93.31	+0.26	+8.43	-8.69	1138
$CdWO_4$	69.31	+6.39	-7.09	+0.70	31
Diamond	68.81	+0.29	-1.60	+1.31	9.2
DPAL Window (averaged)	98.42	+10.33	+6.00	-16.33	3564
Fused Silica	91.75	-0.15	+0.75	-0.60	200
$KTaO_3$	71.16	+0.24	-3.16	+2.92	49
$LaAlO_3$	62.03	-11.38	+0.91	+12.29	45
LYSO	84.94	+0.95	-1.95	+1.00	14
MgO	86.48	+0.47	+0.36	-0.11	10
$RbTiOAsO_4$ (RTA)	83.21	SAMPLE DESTROYED IN REACTION			
$RbTiOPO_4$ (RTP)	82.07	SAMPLE DESTROYED IN REACTION			
Schott 8436	81.01	+0.05	+3.27	-3.33	3472
Sapphire	85.48	+0.41	-0.35	-0.06	25
Spinel	83.71	+1.24	-1.28	+0.04	10
$SrTiO_3$	71.30	+0.46	-0.40	-0.06	91
TAFD-40	81.11	-4.19	+5.24	-1.05	1064
ThO_2	51.78	NO DATA		+37.71	105
Y_2O_3	63.57	+4.86	-4.22	-0.64	59
ZrO_2	62.74	+0.08	+1.90	-1.98	50

CHAPTER 7: DISCUSSION

This Section will discuss the data collected and presented in Chapter 6 and make interpretations thereof. Based on the data collected a recommendation will be made as to what material(s) to pursue for fabrication of DPAL windows and atomic clock vapor cells. Additionally, a brief discussion of future work needed to take the materials found resistant to alkali diffusion and turn them into viable windows and cells will be presented in this final Chapter.

7.1 Conclusions from Data

7.1.1 Effects of Exposure Time on Diffusion

The length of time, unsurprisingly, has a distinct effect on the amount of diffusion in a given sample. In an effort to be determine exactly how Rb diffusion varied with exposure time, a fused silica substrate was included in most runs as a control. ToF-SIMS depth profiles were conducted on these substrates after they were exposed to Rb for varying amounts of time. Figure 35 shows three exposure times with their respective Rb diffusion depths. The most consistent and effective diffusion studies occurred with a 100 °C temperature gradient with the Rb source at ~ 550 °C and the sample maintained at 450 °C. Other variations of the temperature gradient were tested, but they were ineffective.

Experiments were conducted for one, seven, and twenty-one days in order to find a suitable duration for exposure experiments. It was found that a one week run was sufficient and longer times did not substantially improve the amount of diffusion into the samples. As such, most experiments were one week long. Optical characterization results varied from one amorphous sample to another amorphous sample. The transmission of the Schott 8436 glass varied some,

showing increases in transmission in some regions of the spectra and decreases in others as shown in Figure 12.

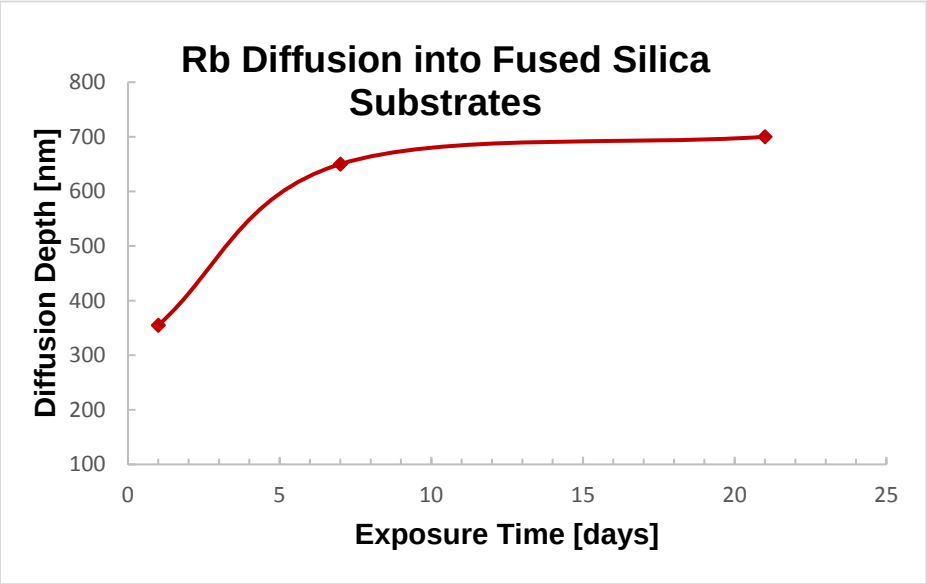

Figure 35. *Rb diffusion into fused silica substrates as a function of exposure time.*

7.1.2 Properties of Materials Studied

Most of the amorphous materials behaved as had been described previously in literature [7, 12]. Rb was able to diffuse deep into these samples with relative ease. Diffusion depths were on the order of microns. This coupled with conflicting data on the maintenance of transmission at the requisite wavelength, i.e., some materials kept their high transmission while others exhibited a dramatic decrease in transmission. It makes most amorphous materials poor candidates to be used as DPAL windows. Also in line with literature [7, 12], crystalline materials resisted diffusion better and in general maintained their optical properties.

There were several materials that did not behave as expected. $LaAlO_3$, for example, exhibited improved optical properties after exposure to Rb. Both spectrophotometric (Figure 23) and ellipsometric (Figure 27) data show significant increase in transmission and reduction in both

index of refraction and extinction coefficient and a therefore decrease in reflection and absorption. These phenomena were observed in several separate experiments that were repeated to confirm these results. As was listed in Table 7, $CdWO_4$ and $KTaO_3$ also exhibited similar behavior. All of these materials have the perovskite crystal structure and the potential significance of this will be discussed in 7.2.3.

7.1.3 Recommendations for Superior Window Materials

Based on the results, ALON, spinel, MgO, and ZrO_2 have been able both maintain high optical transmission while also resisting the diffusion of Rb. It is for these reasons that these materials should be tested more aggressively to determine if they can be used in developing atomic physics systems, DPALs in particular. The next step in this process will be addressed in 7.2.

7.2 Future Work

While this research effort has made headway on the issue of alkali damage and degradation for atomic physics-based systems, there is still more work to be done. The field of candidate materials has been narrowed based on literature and experimental results, but the optimal material still needs to be identified. This section will detail a path forward for future research on the issues that still need to be addressed. Additionally, a more in depth commentary on the phenomena regarding the improvements in transmission observed in $KTaO_3$, $LaAlO_3$, and $CdWO_4$ will be presented.

7.2.1 Atomic Clock Vapor Cell Research

A cell made of cubic zirconia (Figure 36) has been fabricated for use as a vapor cell for Sr-based atomic clocks that are currently under development [4]. Cubic zirconia was selected due to its ability to resist Rb diffusion well while maintaining its optical properties and withstand high

temperatures. It is believed that these traits will also be true for Sr vapor, especially considering that Sr is a slightly larger and less reactive element than Rb.

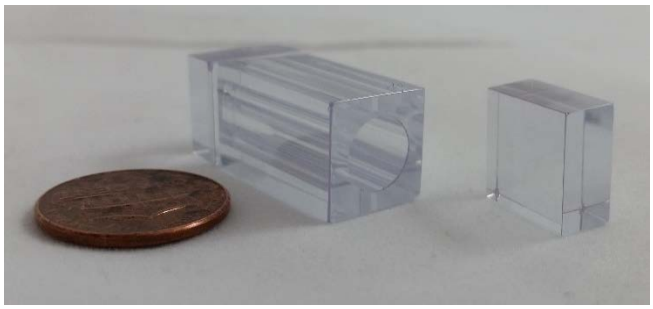

Figure 36. *A vapor cell fabricated out of cubic zirconia.*

7.2.2 DPAL Window Research

The immediate next step for this research regarding DPAL windows is to analyze the ability of these windows to withstand high energy laser radiation. To do this, plans being developed to irradiate exposed and unexposed samples of ALON, spinel, MgO, and ZrO_2 to a high energy laser and through both visual inspection and an IR camera, the effects of heat buildup. If the materials can withstand high energy laser radiation after having been exposed to Rb, then a real window may be prototyped.

Another hurdle for fielding these materials involves the ordinary transmission of the materials chosen. The materials recommended above, as shown in Table 7, do not inherently have optics grade (<99%) transmission. This can be addressed, as was mentioned earlier, anti-reflective coatings were employed to maximize transmission of DPAL windows. It was shown, however, that the Rb had a propensity to not only diffuse through these coatings but also to generate accumulation of material from these AR coatings at the interfaces. This is likely to create a myriad

of problems when attempting to pass high energy laser radiation through. It should be noted, however, that something must be done to improve the transmission of some of the materials used in this study as transmission if often not nearly where it needs to be for high energy laser systems. An alternative to AR coats exists that will eliminate the need for coating a window with different, less alkali resistant materials. This alternative is known as a motheye coating or surface.

Motheye surfaces have been shown to dramatically improve the transmission of window materials. A prime example of such an improvement involves the addition of a motheye surface to a diamond laser window. The laser used was a CO_2 laser that emitted at 1064 nm [52]. The diamond window's transmission at the wavelength, however, was approximately only 70%. After a motheye surface was added to the faces of the laser window, the transmission increased to over 99% [52]. Because of the effectiveness of motheye surfaces and the inherent problems associated with AR coatings in the harsh DPAL gain cell environments, it is proposed that if a material whose transmission is not acceptable for laser window use, but resists alkali diffusion well a motheye surface should be applied to improve transmission instead of more conventional AR coatings.

Another aspect of the DPAL research that could play a crucial role in the damage of window material, is the breakdown of the hydrocarbon. There is both visual and surface evidence that on the surface of the DPAL windows there is a C based soot that deposits on the window surfaces. This soot is likely capable of absorbing some of the DPAL beam which in turn generates localized heating that could lead to the etching of the DPAL windows. Further research should be done in order to ascertain whether the breakdown of the hydrocarbon in the DPAL gain medium is a more significant factor leading to deterioration of DPAL windows than the diffusion of Rb. This research has shown, however, that Rb diffusion by itself does alter the optical properties.

7.2.3 Perovskite Structured Materials

Because of the unexpected improvements in $LaAlO_3$, $CdWO_4$, and $KTaO_3$, further research should be conducted to ascertain what physical mechanism causes this improvement. It is currently unknown at this time whether the changes in optical properties occur due to heating, the diffusion of Rb into the material, or some combination thereof. Simple experiments can be conducted to determine what the cause of these changes, namely, heating the materials to similar temperatures and then analyzing their optical properties. Additionally, crystallographic techniques such as X-ray diffraction spectroscopy can afford insight to a change in crystal structure (if any) before and after exposure to Rb.

REFERENCES

[1] T. P. Heavner, S. Jefferts, E. A. Donley, and T. E. Parker, "NIST F1: Recent Improvements and Accuracy Evaluations," *Metrologia*, no. 42, p. 411, 2005.

[2] H. Kissel, B. Köhler, and J. Biesenbach, "High-power Diode Laser Pumps for Alkali Lasers (DPALs)," DILAS Diodenlaser GmbH, Mainz, 2012.

[3] C. Salomon, Y. Sortais, S. Bize, M. Abgrall, S. Zhang, C. Nicolas, C. Mandache, P. Lemonde, G. Santarelli, A. Clairon, N. Dimarcq, P. Petit, A. Mann, and A. C. S. Luiten, "Cold Atom Clocks," in *XVII International Conference ICAP 2000*, 2001.

[4] A. D. Ludlow, T. Zelevinsky, G. K. Campbell, S. Blatt, M. M. Boyd, M. H. G. de Miranda, M. J. Martin, J. W. Thomsen, S. M. Foreman, J. Ye, T. M. Fortier, J. E. Stalnaker, S. A. Diddams, Y. Le Coq, Z. W. Barder, N. Poli, and N. D. Lemke, "Sr Lattice Clock at 10^{-16} Fractional Uncertianty by Remote Optical Evaluation with Ca Clock," *Science,* vol. 319, p. 1805, 2008.

[5] L. Quarrie, "The Effects of Atomic Rubidium Vapor on the Performance of Optical Windows in Diode Pumped Alkali Lasers (DPALs)," *Optical Materials*, vol. 35, p. 843, 2012.

[6] W. Krupke, "Diode-pumped Alkali Lasers Aim for Single-aperture Power Scaling," SPIE, 2008.

[7] J. Lau, "Transparent Glass-ceramics and Interaction with Alkali Metal Vapours," 1980.

[8] A. Tilocca, "Sodium Migration Pathways In Multicomponent Silicate Glasses: Car–Parrinello Molecular Dynamics Simulations," *The Journal of Chemical Physics,* vol. 133, p. 014701, 2010.

[9] C. Volk, R. Frueholz, T. English, T. Lynch, and W. Riley, "Lifetime and Reliability of Rb Discharge Lamps for use in Atomic Frequency Standards," Space Division Air Force Systems Command, Los Angeles, 1984.

[10] K. Liu and A. Mukhopadhyay, "Alkali-Silica Reaction in a Form of Chemical Shrinkage," *Civil Engineering and Architecture*, vol. 2, p. 235, 2014.

[11] C. Ferraris, "Alkali-Silica Reaction and High Performance Concrete," Building and Fire Research Laboratory, NIST, Gaithersburg, 1995.

[12] J. Cheng, W. Liang, Y. Hu, and G. Chen, "Development of a New Alkali Resistant Coating," *Journal of Sol-gel Science and Technology,* vol. 27, p. 309, 2003.

[13] A. Paul, "Chemical Durability of Glasses; a Thermodynamic Approach," *Journal of Material Sciences,* vol. 12, p. 2246, 1977.

[14] SCHOTT North America, "SCHOTT North America," [Online]. [Accessed 23 January 2017].

[15] Y. V. Lipatov, S. I. Gutnikov, M. S. Manylov, and B. I. Lazoryak, "Effect of ZrO_2 on the Alkali Resistance and Mechanical Properties of Basalt Fibers," *Inorganic Materials,* vol. 48, p. 751, 2012.

[16] D. Gray, American Institute of Physics Handbook, McGraw-Hill Inc., 1972.

[17] Hoya Group Optics Division, "Hoya Datasheet," 29 September 2016. [Online]. Available: www.hoya-opticalworld.com/english. [Accessed 2 April 2017].

[18] R. C. Weast, CRC Handbook of Physical Chemistry, Cleveland: CRC Press, 1978.

[19] Z. Ji, H. Ni, L. Yuan, J. Chen, and S. Wang, "Correlation Between Light Response Uniformity and Longitudinal Transition in 600 nm BGO Crystals," *Key Engineering Materials,* vol. 633, p. 277, 2015.

[20] R. Mao, C. Wu, L. Dai, and S. Lu, "Crystal Growth and Scintillation Properties of LSO and LYSO Crystals," *Journal of Crystal Growth,* vol. 368, p. 97, 2013.

[21] R. C. Linares, "Growth and Properties of CeO_2 and ThO_2 Single Crystals," *Journal of Physics and Chemistry of Solids,* vol. 28, p. 1285, 1967.

[22] N. S. Prasad, W. C. Edwards, S. B. Trivedi, C. Wang, J. Kim, U. Hommerich, V. Shulka, R. Sadangi, and B. H. Kear, "Recent Progress in the Development of Neodynium-doped Ceramic Yttria," *IEEE Journal of Selected Topics in Quantum Electronics,* vol. 13, p. 831, 2007.

[23] Q. Xiao, C. Xu, S. Shao, J. Shao, and Z. Fan, "Y_2O_3 Stabilized ZrO_2 Thin Films Deposited by Electron-Beam Evaporation: Optical Properties, Structure and Residual Stresses," *Vacuum,* vol. 83, p. 366, 2008.

[24] Surmet, "Technical Data - ALON Optical Ceramic," Surmet Corporation, Burlington.

[25] Laser Crystal, "Cristal-laser," [Online]. Available: www.cristal-laser.com/UserFiles/File/brochures-techniques/rtp.pdf. [Accessed 04 May 2017].

[26] V. A. Strelsov, J. Nordborg nee Almgren, and J. Albersson, "Synchrotron X-ray Analysis of $RbTiOAsO_4$," *Acta Crystallographica Section B,* vol. 56, p. 785, 2000.

[27] Z. G. P. K. Zhong, D. L. Loiacono, and G. M. Loiacono, "The Thermal Expansion and Stability of $KTiOAsO_4$ and Related Compounds," *Thermochimica Acta,* vol. 234, p. 255, 1994.

[28] G. D. Stucky, L. F. Phillips, and T. E. Geir, "The Potassium Phosphate Structure Field: A Model for New Nonlinear Optics Materials," *Chemistry of Materials,* vol. 1, p. 492, 1989.

[29] J. Han, Y. Liu, and D. Nei, "Flux Growth and Properties of $RbTiOAs_4$ (RTA) Crystals," *Journal of Crystal Growth,* vol. 128, p. 846, 1993.

[30] A. S. Lyakhov, A. F. Selevich, and A. I. Verenich, "Ctrystal Structure of Rubidium Titanyl Phosphate a-$RbTiOPO_4$," *Russian Journal of Inorganic Chemistry,* vol. 38, p. 1121, 1993.

[31] Lasertec, 2005. [Online]. Available: lcoptical.com/RTP/RTP.html. [Accessed 04 May 2017].

[32] A. Meldrum, L. A. Boatner, W. J. Weber, and R. C. Ewing, "Amorphization and Recrystallization of the ABO_3 Oxides," *Journal of Nuclear Materials,* vol. 300, p. 242, 2002.

[33] L. Bardelli, M. Bini, P. G. Bizzeti, L. Carraresi, F. A. Danevich, T. F. Fazzini, B. V. Grinyov, N. V. Ivannikova, V. V. Kobychev, B. N. Kropivyansky, P. R. Maurenzig, L. L. Nagornaya, S. S. Nagorny, A. S. Nikolaiko, A. A. Pavlyuk, D. V. Poda, I. M. Solsky, M. V. Sopinskyy, Yu. G. Stenin, F. Taccetti, V. I. Tretyak, Ya. V. Vasiliev, and S. S. Yurchenko, "Further Study of $CdWO_4$ Crystal Scintillators as Detectors for High Sensitivity 2B Experiments: Scintillation Properties and Pulse-shape Discrimination," *Nuclear Instruments and Methods in Physics Research,* vol. 569, p. 743, 2006.

[34] S. C. Sabhrwal and Sangeeta, "Study of Growth Imperfections, Optical Absorption, Thermoluminescence and Radiation Hardness of $CdWO_4$ Crystals," *Journal of Crystal Growth,* vol. 200, p. 191, 1999.

[35] B. Union, "Buoptics," [Online]. Available: buoptics.com/upfiles/word/20108231748327895.pdf. [Accessed 04 05 2017].

[36] CrysTec, "CrysTec," KristallTechnologie GmbH, [Online]. Available: www.crystec.de/laalo3-e.html. [Accessed 2017].

[37] X. H. Zeng, L. H. Zhang, G. J. Zhao, J. Xu, Y. Hang, H. Y. Pang, M. Y. Jie, C. F. Yan, and X. M. He, "Crystal Growth and Optical Properties of $LaAlO_3$ and Ce-doped $LaAlO_3$ Single Crystals," *Journal of Crystal Growth,* vol. 271, p. 319, 2004.

[38] E. A. Philip and H. R. Taft, "Optical Properties of Diamond in the Vacuum Ultraviolet," *Physical Review,* vol. 127, p. 159, 1962.

[39] E. 6, "Enable Extreme Performance Photonic," De Beers Group, Santa Clara.

[40] H. G. Tompkins and W. A. McGahan, Spectroscopic Ellipsometry and Reflectometry, New York: John Wiley & Sons, inc., 1999.

[41] P. S. Bagus, E. S. Ilton, and C. J. Nelin, "The Interpretation of XPS Spectra: Insights Into Mmaterials Properties," *Surface Science Reports,* vol. 68, p. 273, 2013.

[42] L. Van Vaeck, A. Adriaens, and R. Gijbels, "Static Secondary Ion Mass Spectrometry: (S-Sims) Part 1. Methodology and Structural Interpretation," *Mass Spectrometry Reviews,* vol. 18, p. 1, 1999.

[43] A. Radionova, I. Filippov, and P. J. Derrick, "In Pursuit of Resolution In Time-of-flight Mass Spectometry: A Historical Perspective," *Mass Spectrometry Reviews,* vol. 35, p. 738, 2015.

[44] L. Van Vaeck, A. Adriaens, and R. Gijbels, "Static Secondary Ion Mass Spectrometry (S-SIMS) Part 2: Material Science Applications," *Mass Spectrometry Reviews,* vol. 18, p. 48, 1999.

[45] R. M. A. Azzam and N. M. Bashara, Ellipsometry and Polarized Light, Amsterdam: North Holland Press, 1977.

[46] A. R. Forouhi and I. Bloomer, "Optical Dispersion Relations for Amorphous Semiconductors and Amorphous Dielectrics," *Physical Review B,* vol. 38, p. 7018, 1986.

[47] A. R. Forouhi and I. Bloomer, "Optical Properties of Crystalline Semiconductors and Dielectrics," *Physical Review B,* vol. 38, p. 1865, 1988.

[48] N. Laidani, R. Bartali, G. Gottardi, M. Anderle, and P. Cheyssac, "Optical Absorption Parameters of Amorphous Carbon Films From Forouhi-Bloomer and Tauz-Lorentz Models: A Comparative Study," *Journal of Phyics,* vol. 20, p. 8, 2008.

[49] E. Stoumbou, I. Stavtakas, G. Hloupis, A. Alexandridis, D. Triantis, and K. Moutzouris, "A Comparative Study on the Use of the extended-Cauchy Dispersion Equation for Fitting refractive Index Data in Crystals," *Optical and Quantum Electronics,* vol. 45, p. 837, 2013.

[50] P. L. Washington, H. C. Ong, and J. Y. Dai, "Determination of the Optical Constants of Zinc Oxide Thin Films by Spectroscopic Ellipsometry," *Applied Physics Letters,* vol. 72, p. 3261, 1998.

[51] G. Franceshinis, "Surface Profilometry as a Tool to Measure Thin Film Stress, A Practical Approach," Rochester Institute of Technology, Rochester, 2005.

[52] M. Peach, "PureOptics has ‘Moth’s Eye’ Design to Cut Reflection Losses, Removing Need for Coatings that Cut Performance," 2015.